UCLouvain

AGRO LOUVAIN

Faculté des bioingénieurs

Spatio-temporal modelling of groundwater resources to improve drought risk assessments

Proposal of indicators for Siliana catchment in Tunisia

Auteur :	Wail Semlali
Promoteur :	Marnik Vanclooster
Lecteurs :	Alice Alonso
	François Jonard
	Slaheddine Khlifi
Année Académique :	2020 - 2021
Study program :	Environmental Bioengineering

List of Figures

List of Tables

Abbreviations

AEI Accumulated Emptying Index.

AFI Accumulated Filling Index.

AI Aridity Index.

ARDD Accumulated Recharge-Discharge Difference.

ARDR Accumulated Recharge-Discharge Ration.

ASCE American Society of Civil Engineers.

CCNUCC Convention Cadre des Nations Unies sur les Changements Climatiques.

CHIRPS Climate Hazards group Infrared Precipitation with Stations.

CLSM Catchment Land Surface Model.

CRED Centre for Research on the Epidemiology of Disasters.

CSR Center for Space Research at University of Texas, Austin.

DEM Digital Elevation Model.

DGRE Direction Générale des Ressources en Eau.

EI Emptying Index.

ELIE Earth and Life Institute.

EMDAT Emergency Events Database.

ESIM Ecole Supérieure des Ingénieurs de Medjez El Bab.

ET Evapotranspiration.

EU European Union.

FAO Food and Agriculture Organization.

FI Filling Index.

GEE Google Earth Engine.

GGDI Grace Groundwater Drought Index.

GIS Geographic Information System.

GLEAM Global Land Evaporation Amsterdam Model.

GRACE Gravity Recovery and Climate Experiment.

GSD Groundwater Storage Deviation.

GSFC Goddard Space Flight Center.

GWI Groundwater Index.

GWSA Groundwater Storage Anomaly.

GZP GeoforschungsZentrum Potsdam.

HRU Hydrological Response Unit.

ICID International Commission on Irrigation and Drainage.

JPL Jet Propulsion Laboratory.

K-S Kolmogorov-Smirnov.

MASCON Mass Concentration blocks.

MLE Maximum Likelihood Estimation.

NASA National Aeronautics and Space Administration.

OSS Observatoire du Sahara et du Sahel.

PDI Percolation Drought Index.

PET Potential Evapotranspiration.

PWM Probability Weighted Method.

RCP Representative Concentration Pathway.

RDD Recharge-Discharge Difference.

RDR Recharge-Discharge Ratio.

RFA-LM Regional Frequency Analysis L-Moments.

SGI Standardized Groundwater Index.

SPEI Standardized Precipitation and Evapotranspiration Index.

SPI Standardized Precipitation Index.

SRTM Shuttle Radar Topography Mission.

SSH Standard Spherical Harmonic.

SWAT Soil and Water Assessment Tool.

TAMSAT Tropical Applications of Meteorology using Satellite.

TWSA Terrestrial Water Storage Anomalies.

UNCDD United Nations Conventions to Combat Desertification.

UNEP United Nations Environment Programme.

USA United State of America.

WBI Wallonie-Bruxelles International.

WCI Water Cycle Generator.

WMO World Meteorological Organization.

Remerciements

Je tiens à remercier avant tout les personnes directement impliquées dans l'écriture de ce mémoire de fin d'étude à savoir mon promoteur le Pr. Marnik Vanclooster et la chercheuse post-doctorale Alice Alonso pour leur suivi régulier, leur disponibilité et leurs précieux conseils tout au long de cette année de mémoire. Je remercie également le Pr. Slaheddine Khlifi de l'ESIM pour ses retours constructifs sur mon travail et la chercheuse Imen El Ghoul pour son soutien, sa patience et sa disponibilité concernant la découverte et l'utilisation du logiciel SWAT+. Je remercie également Jimmy et Manon pour leur solidarité.

Je remercie Gabriel, Lucas, Hélène et Martin pour leur agréable présence durant nos sessions de travail et leur aide lors des questionnements et problèmes techniques auxquels j'ai été confronté, ainsi qu'à tous les autres qu'il serait trop long de citer ici et qui ont été là pour moi.

Je remercie mes colocataires Antoine, Dorian, Lucia, Lyssia, Odile et Victoria pour leurs encouragements, leur bonne humeur et leur présence lorsque le manque d'inspiration et d'énergie se faisait ressentir. Les soirées passées dans le salon, les chaleureux repas du soir et les virées crème glacées égayèrent mes journées et soirées, ces moments de lâcher prise si nécessaire en ces périodes troublantes. Je tiens à remercier en particulier Odile pour ses conseils enrichissants, ses réflexions pertinentes et rassurantes faces aux difficultés et incertitudes auxquelles j'ai été confrontés.

Enfin Je remercie mes frères et soeurs Chadi, Inare et Maher ainsi que mes parents Ahmed et Badia que je porte dans mon coeur. Leur soutien, leurs encouragements et leur curiosité vis-à-vis de mes recherches durant cette année ainsi que durant toutes ces années d'études. Leur présence a été pour moi une source intarissable d'énergie et de réconfort.

Contents

1 Introduction

Tunisia is the Maghreb country with the most severe water deficit. It exhibits an average availability of fresh water below 500m^3/year/inhabitant that is considered as a threshold of absolute water scarcity (Rapport national du secteur de l'eau, 2019). In addition, climate change projections for 2050 according the Representative Concentration Pathway (RCP)'s 4.5 and 8.5 emission scenario predict an increase of respectively 1 to 1.8 C° and 2 to 2.3 C° for Tunisia compared to the pre-industrial society. These scenarios suggest also a decrease in average annual precipitation and longer extreme heat events (CCNUCC, 2018). Tunisia is therefore situated in a hotspot region affected by climate change. Climate change reduces considerably availability of water resources, affecting the resilience of the tunisian society. In this context, Tunisia is expected to strengthen its drought management strategy. Drought management strategies encompass different components, such as drought monitoring, drought adaptation and mitigation.

With respect to drought monitoring, most monitoring systems concentrate primarily on meteorological drought. Different meterological drought indices are proposed that directly can be calculated from monitored meteorological data. In other cases, hydrological and agronomical drought indices are monitored that incoporate the monitoring of water storage in soil, rivers, lakes and/or the monitoring of vegetation vigour. In yet other cases, drought indices can be produced that consider the availability of water in the groundwater reserves. For these latter cases, operational groundwater monitoring is required.

With respect to adaptation strategies, strategies include the development of institutional and physical infrastructure to cope with drought. With respect to physical infrastructure, water conservation measures can be proposed such as the creation of retention bassins, surface water reservoir and groundwater reinfiltration. The use of groundwater reservoirs for implementing water conservation is attractive, since it fully exploits natural resources to store the water, it implies low cost infrastructure (infiltration basin) and it protects the water against excessive evaporation losses. The groundwater exploitation potential in Tunisia is estimated at 2190 Mm^3 (DGRE, 2018), which represents more or less 45% of total freshwater potential of the country. The groundwater component is therefore important to be considered in the drought management strategy of Tunisia.

In this master's thesis, the role of the groundwater component in drought assessment methodologies is further elaborated. The general objective of the master thesis is to propose and test a methodology that integrates groundwater resources in a drought diagnosis. This would allow for a more holistic assessment of the

impact of drought on available water resources. The aim is also to ensure that the methodology can become operational for water resource management in Tunisia. The methodology should therefore be based on data coming from existing monitoring infrastructure.

To reach these objectives, a research action is implemented using the Siliana catchment as case study. The Siliana catchment is a tributary of the Medjerda river which is the largest permanent river of the country. The catchment is situated in the northern part of Tunisia. The research action is structured along 4 different items.

Firstly, a literature review is made on drought assessment methodologies, with the emphasis on methodologies that allow the integration of groundwater resources in drought diagnostics.

Secondly, droughts are assessed using three different methods that will be compared. The first methodology is a meteorological based reference methodology. In this method, satellite based precipitation data are used to evaluate a meteorological drought indicator (the SPI indicator). The second methodology is a hydrologeological oriented methodology based on groundwater body observations. A diagnostic of in situ available piezometric data is made for the study area that allows for drought assessment. This method allows determining the spatio-temporal and technical limitations of drought dynamics analysis that are based on available groundwater data. For the third method, a hydrological model is implemented for the Siliana catchment with Soil and Water Assessment Tool (SWAT)+ and QGIS. This model allows assessing water infiltration, and hence groundwater recharge.

This master's thesis is developed within the SMART Medjerda project (2019-2023), implemented by Ecole Supérieure des Ingénieurs de Medjez El Bab (ESIM) and Earth and Life Institute (ELIE) UCLouvain and supported by Wallonie-Bruxelles International (WBI). The aim of the SMART Medjerda project is to strengthen the capacity of Tunisian actors in the area of water management and hence increase the resilience of water management in a changing climate environment.

2 State of the art

2.1 Drought definition

Drought is considered as one of the most complex natural hazards due to its complicated nebulous features and lack of universal definition (Wilhite et al., 2007). The beginning, the end and the spatial distribution of a drought episode are not explicit (Wilhite et al., 2007; Hisdal and Tallasken, 2000). Also, the intensity depends on the context where it occurs (Gordon, 1992). It depends on the climatic regime, the vulnerability of the region and the societal risk management skills of humans in the considered region. It's also the most common natural disaster affecting people, with 69.1% of all disasters attributed to drought (Guha-Sapir et al., 2017).

Some other phenomenona can be mistakenly attributed to drought and it is important to distinguish them before.

2.1.1 Aridity

Aridity is defined as a permanent moisture deficit under normal conditions (Middleton and Thomas, 1997) where drought is a temporary phenomenon represented by a water deficit (Maliva and Missimer, 2012). Aridity is therefore climatologically related to water availability and different specific definitions are available to define it (Spinoni et al., 2015). Using the mean annual precipitation, for instance, aridity can be classified into four groups (See table 1) (Holzapfel, 2008).

	Precipitation
Extreme arid	$P <$ 60-100 mm
Arid	60-100 $< P <$ 150-250 mm
Semi-arid	150-250 $< P <$ 250-500 mm
Mesic	$P >$ 500 mm

Table 1: Aridity classes based on annual precipitation mean (mm)

Nonetheless, to get a more precise classification, the Aridity Index (AI) suggested by the Food and Agriculture Organization (FAO) takes into account as well the Potential Evapotranspiration (PET) as the precipitation during 30 years to evaluate aridity (see equation 1) (Spinoni et al., 2014).

$$AI = \frac{\sum_{i=1}^{30}(\frac{P_i}{PET_i})}{30} \quad (1)$$

where :

- i : the specific year;
- P_i : the precipitation for a given year (mm); and
- PET_i : the potential Evapotranspiration for a given year (mm).

Four classes are identified for dryland regions (See table 2)

	Aridity index
Hyper arid	AI $<$ 0.05
Arid	0.05 $<$ AI $<$ O.2
Semi-arid	0.2 $<$ AI $<$ 0.5
Dry subhumid	0.5 $<$ AI $<$ 0.65

Table 2: Classes of climates based on AI

2.1.2 Desertification

The first time this concept appeared was in 1927 by Louis Lavauden and popularized by Aubréville in 1949 (Darkoh, 2003). Used to define the extreme environmental degradation of tropical and subtropical forest in Africa, the signification of this word was widely debated during the second part of the twentieth century (Verstraete, 1986).

The United Nations Conventions to Combat Desertification (UNCDD) proposes the following definition (UNCCD, 2017):

"Land degradation in arid, semi-arid and dry sub-humid areas resuls from various factors, including climatic variations and human activities."

Following this definition, we can see that desertification depends partly on human pressure. Nonetheless, notions like reversibility, location, rate of progression, causes and cures pointed out by Verstraete (1986) must be always kept in mind when desertification is discussed.

2.1.3 The drought concept

Despite the lack of a universal definition for drought, four aspects outline the drought concept (Funk and Shukla, 2020):

- **A slow-onset phenomenon**. This aspect provides the possibility to implement early warning system but complicates the identification of switch period to drought situation.

- **The multidimensionality**. This aspect aims to highlight the magnitude of the phenomenon through 3 criteria (Sheffield and Wood, 2012; Wilhite and Glantz, 1985):

  - *Intensity*
  - *Duration*
  - *Extent*

  The timing when drought occurs will also influence the vulnerability of societies and ecosystems to drought (war, economic crisis, water pollution, etc).

- **The multidisciplinary and multisectoral nature of droughts**.

  Four types of drought are commonly developed (OSS, 2008):

  - *Meteorological drought.* This type of drought is based on the abnormal decrease of rainfall in a certain period of time relatively to historical records. For the historical records, at least thirty years of data should be considered;
  - *Agronomic drought.* This type is based on soil water humidity deficit;
  - *Hydrological/hydrogeological drought.* The hydrological/hydrogeological drought is based respectively on surface and groundwater deficit; and
  - *Socio-economic drought.* Such drought type reflects the consequences of the other drought types on the organization of human society.

  Those types of drought can be concomitant but the first phenomenon is generally always a meteorological drought.

- **The complexity of drought impacts**.

  With respect to impacts, droughts can affect different sectors :

  - The *environmental sector* by damaging wildlife habitats, fauna and flora, water quality etc.;

- The *economic sector* by direct losses for agriculture, industries, energy production etc.;
- The *social sector* by water and food shortages, food price increase, conflicts etc.

Using these definitions, descriptive tools are necessary to cope with the complexity of drought.

2.2 Drought diagnostic tools

2.2.1 Meteorological drought

- Standardized Precipitation Index (SPI)

  Developed by (McKee et al, 1993), the SPI is based on the normalization of a cumulative probability of observed monthly precipitation for a given month. At least 30 years of continuous monthly precipitation data are needed to have a reliable index and the longer the historical data, the better the reliability (Guttman, 1994). The two assumptions for a precipitation-based index are (Vicente-Serrano et al., 2010) :

  - The variability of precipitation is more important and more determinant than other variables such as temperature and evapotranspiration.
  - The other variables do not show important temporal dynamics which allows to neglect them.

  SPI is generally calculated by a two-parameter probability distribution and the most suitable is the Gamma distribution (Guttman, 1999) but other distributions are possible like the Poisson-Gamma distribution (Lana et al., 2001) or a non-parametric distribution (Kumar et al., 2016). The SPI index classify the rarity of a precipitation episode in a scale that can take both negative and positive values. It represents respectively dry and wet conditions. The intensity of a drought or a flood episode is determined by the deviation of SPI from the median value shown on Table 3 (McKee et al, 1993).

  SPI can use different time windows to evaluate droughts (Edwards, 1997). For example, to calculate a 3-month SPI for january, the range of observed precipitation will take november, december and january precipitation data into account. The length of the time window will determine some specific drought types:

  - the 3-month SPI is used to assess a short-term or seasonal drought;

Classes	SPI
Extremely wet	> 2.0
Very wet	1.99 to 1.49
Moderately wet	1.49 to 1.0
Near normal	-0.99 to 0.99
Moderately dry	-1.0 to -1.49
Severely dry	-1.49 to -1.99
Extremely dry	$<$ -2.0

Table 3: SPI values and intensity of drought/wet episodes (McKee et al, 1993)

- the 12-month SPI is used for evaluating an intermediate-term drought; and
- the 48-month is used for assessing long-term droughts.

The cumulative probability of historical monthly rainfall records is standardized to calculate values shown on Table 3. The SPI calculated with different time windows can identify different drought types. For instance the 12-month SPI may be more indicative for hydrological droughts (WMO, 2012).

Yet, the use of long term window based SPI indices may become problematic to assess hydrogeological drought. Kumar et al., (2016) for instance assessed hydrogeological droughts in South Germany and the Netherlands, using data from more than 2000 wells that did not exhibit significant anthropogenic influence. Use was made of Standardized Groundwater Index (SGI) to assess hydrogeological drought. Sheffield et al. (2004) introduced the quantile-based index SGI for representing anomalies in the groundwater heads. Values below 0.2 suggest a hydrogeological drought episode (Sheffield et al., 2004; Andreadis et al., 2005; Vidal et al., 2010; Samaniego et al., 2013; Kumar et al., 2016). The SGI can be compared with the long time window SPI. Based on such analysis, Kumar et al., (2016) suggests that different time spans for evaluating SPI must be considered for different locations due to the variability of (hydro)geological characteristics of each groundwater well.

One of the main criticism concerning the SPI is the univariate approach, ignoring the role of other variables like temperature, evapotranspiration, wind speed and soil water holding capacity in drought evaluation (Vicente-Serrano et al., 2010). Nonetheless, rainfall deficit is the reference variable for all types of drought (Glantz and Wilhite, 1985). Yet, one of the main advantages is that reliable long term rainfall observations become now available at the

global scale (Heim, 2002), allowing for a robust assessment of global droughs. Hence, SPI remains the primary indicator to be evaluated for droughts.

- Standardized Precipitation and Evapotranspiration Index (SPEI)

  Eigthy % of rainfall is consumed by evapotranspiration (Abramopoulos et al., 1988). Hence introducing knowledge about the evapotranspiration allows improving assessing drought.The Standardized Precipitation and Evapotranspiration Index (SPEI) allows doing this. The SPEI is built on the same principle of SPI, but instead of monthly precipitation, the difference between rainfall and Potential Evapotranspiration (PET) is calculated (Vicente-Serrano et al., 2010).

$$D_i = P_i - PET_i \tag{2}$$

  with :

  - i : a specific month;
  - P_i : the precipitation for a given month i;
  - PET_i : the potential evapotranspiration for a given month i;

  The physically based method of Penman-Monteith is considered as the standard approach for PET calculation by Food and Agriculture Organization (FAO), International Commission on Irrigation and Drainage (ICID) and American Society of Civil Engineers (ASCE). The parameters that are needed are solar radiation, temperature, wind speed, and relative humidity (Vicente-Serrano et al., 2010).

  Nonetheless, for regions where those parameters are not available, the difference between simple and complex potential evapotranspiration method for assessing SPEI is not significant (Mavromatis, 2007). Therefore the SPEI proposed by (Vicente-Serrano et al., 2010) use the simplified method elaborated by Thornthwaite (1948) for evaluating SPEI (see Equation 3) :

$$PET = 16K(\frac{10T}{I})^m \tag{3}$$

  with :

  - K : the correction coefficient computed as a function of the latitude and month;

- T : the monthly mean temperature [C°]
- I : the heat index calculated as the sum of 12 monthly index values i;
- $i = (\frac{T}{5})^{1.514}$; and
- m = 6.75 * 10^{-7} * I^3 - 7.71 * 10^{-5} * I^2 + 1.79 * 10^{-2} * I + 0.492

The SPEI, unlike the SPI, requires a three-parameter distribution model to take into account negative values from the water balance calculated via equation 2. The most suitable fitting curve was shown to be a log-logistic distribution (Vicente-Serrano, 2010).

Vicente-Serrano (2010) have shown that SPEI identifies the same drought episodes than SPI, which suggests that SPEI is an efficient drought indicator. In the context of global warming and increased temperature scenarios, the SPEI is however relevant in order to assess the severity of drought episodes.

2.2.2 Hydrogeological drought

The annual global groundwater abstraction of about 1000 km^3/year estimated in 2010, is considered as the most extracted raw material on Earth (Margat and van der Gun, 2013). Nonetheless, the limitation of groundwater data induces difficulties to implement efficient groundwater resources (Vrbo and Lippanen, 2007). Yet, the efficient monitoring of groundwater dynamic is essential for sustainable water resources management, especially for countries where drought episodes often occur (Aghakouchak et al., 2014).

- Simple and in situ indices

Six indices have been proposed by (Van Camp et al., 2010) in order to assess the groundwater depletion and hence hydrogeological drought (See Table 4)

Indicator	Explanation	Definition
FI	Filling Index	$FI_i = \frac{PL_i - PLmin}{PL_{max} - PL_{min}}$
AFI	Accumulated FI	$AFI = \sum_{i=1}^{m} FI_i$
RDR	Recharge–Discharge Ratio	$RDR = \frac{RECH_i}{DISCH_i}$ 1
ARDR	Accumulated RDR	$ARDR = \sum_{i=1}^{m} RDR_i$
RDD	Recharge-Discharge Difference	$RDD = RECH_i - DISCH_i$
ARDD	Accumulated RDD	$ARDD = \sum_{i=1}^{m} RDD_i$

Table 4: Simple indices for groundwater depletion assessment (Van Camp et al., 2010)

where :

- FI_i : Filling index for month i;
- PL_i : Piezometric level (m) for month i;
- PL_{min} : Minimum piezometric level (m) for the considered time series;
- PL_{max} : Maximum piezometric level (m) for the considered time series;
- $RECH_i$: Aquifer recharge (m^3/day) in month i; and
- $DISCH_i$: Aquifer discharge (m^3/day) in month i

The two first indices only need piezometric time series, which is easily built in order to get a quick view on groundwater evolution. The others need a more complex approach.

In the Shahrekord plain basin in Iran, (Van Camp et al., 2010) used soil moisture balance approach with the method proposed by (Thornthwaite and Mather, 1955, 1957) and implemented into the program WATBUG (Willmott, 1977) to calculate recharge.

For discharge, irrigation data were used. Streamflow out of the basin was considered negligable. The aquifer is located in a nearly closed basin which implies low lateral inflow and outflow. The storage variation therefore depends mainly on exploitation rate and rainfall recharge. In this case, the substratum of the aquifer was made of limestone.

Fifteen wells with data series from 1984 to 2003, and four beginning in 1987, were used to calculate the FI and AFI indices. The indices show a good correlation with the accumulated change in groundwater storage as modeled with the physical based numerical groundwater flow model MODFLOW. The best correlation values were obtained for ARDR and ARDD. Nonetheless, the same recharge estimation and discharge records were used for implementing the model and calculate the indices, which partially enhanced the correlation observed between the accumulated change in storage calculated by the model and the ARDR and ARDD.

Another in situ indicator called Groundwater Index (GWI) is proposed by Thomas et al. (2017). It is based on spatio-temporal approach and the deseasonalization method of (Li and Rodell, 2015). The monthly groundwater storage observations for a specific well are spatialized by Thiessen polygon analysis following equation 4. The regionalised groundwater storage is calculated for a given month:

$$GWS_t = \frac{\sum_{i=1}^{n}(A_i \cdot GW_{t_i})}{\sum_{i=1}^{n} A_i} \tag{4}$$

with :

- i : a specific month;
- GWS_t : Regionalised groundwater storage depending on time (t) [m]; and
- A_i : Area of the Thiessen polygon for well i;

The local groundwater storage term (GW_{t_i}) can be calculated via equation 5 and depends on specific yield (S_y) of the well. This latter parameter is determined by soil features and water level observed in wells in meter (h) (Thomas et al.,2017 ; Frappart et al.,2018).

$$GW = S_y \cdot h[m] \tag{5}$$

The seasonality is removed by equation 6 and the GWI is normalized by time series mean ($\overline{X_t}$) and standard deviation (s_{X_t}) via equation 7:

$$X_t = GWS_{t_m} - \overline{GWS_{t_m}} \tag{6}$$

$$GWI_t = \frac{X_t - \overline{X}_t}{s_{X_t}} \tag{7}$$

Li and Rodell (2014) derived the GWI from in situ data and from the Catchment Land Surface Model (CLSM). Monthly groundwater storage data were calculated via Princeton meteorological dataset with a time resolution of 3 hours and spatial resolution of 1° for precipitation, wind speed, solar radiation, surface air temperature, surface pressure and relative humidity from 1948 to 2010 (Sheffield et al., 2006). Results have shown strong correlation between in situ and CLSM model-based GWI and also a strong correlation for both to the SPI-12 and SPI-24, showing similar degrees of severity for drought events.

The last index presented is the Standardized Groundwater Index (SGI) proposed by Bloomfield and Marchant (2013). It is based on the same approach than SPI but instead of precipitations, monthly observed groundwater levels are used. The first statement is the difficulty to find a theoretical distribution to fit groundwater levels. In the study of Bloomfield and Marchant (2013), normal score transformation is used on 14 sites accross the United Kingdom. Unlike SPI, SGI cannot be calculated for different accumulation period since

groundwater levels are continuous variables. Furthermore, SPI is a drought index which is not influenced by geographical differences while SGI is highly affected by location. Autocorrelation of SGI time series is applied for each site to quantify groundwater drought. A cross correlation is applied between both indices to study the potential temporal lag and maximum cross correlation scores (0.87) is attained for SPI-10, with a temporal lag of one month and the minimum (0.70) is attained for SPI-7 and without temporal lag. The study concludes that SGI identifies well groundwater drought with regard to previous drought episodes listed in the country.

- Satellite-based index

  The observation of water storage dynamics at large scales by remote sensing satellite which was considered pertinent by (Rodell and Famiglietti, 1999; Wahr et al., 2006), is better monitored since the launch of Gravity Recovery and Climate Experiment (GRACE) satellite by the National Aeronautics and Space Administration (NASA) in 2002. The service was stopped due to battery issues in 2017. Chen et al. (2020) and Rowlands et al. (2005) consider that it can be an additional data source for drought monitoring. The GRACE satellites measured the variation of Earth gravity field and related this variation to variation of global water storage (Landered and Swenson, 2012; Long et al., 2014; Sinha et al., 2019). GRACE satellites provided a global monthly estimation of Terrestrial Water Storage Anomalies (TWSA) based on snow water, surface water, soil water, canopy water, and groundwater (Scanlon et al., 2018) (see equation 4).

$$TWSA = SnWS + CWS + SWS + SMS + GWS \tag{8}$$

  with :

  - $TWSA$: Terrestrial Water Storage;
  - $SnWS$: Snow Water Storage;
  - CWS : Canopy Water Storage;
  - SWS : Surface Water Storage;
  - SMS : Soil Moisture Storage;
  - GWS : Groundwater Storage;

  Two approaches are proposed for calculating TWSA[2] (see figure 1): the Standard Spherical Harmonic (SSH) approach with three processing systems

[2] $https://grace.jpl.nasa.gov/data/choosing-a-solution/, 06/06/2021$

largely used (Jet Propulsion Laboratory (JPL); Center for Space Research at University of Texas, Austin (CSR); GeoforschungsZentrum Potsdam (GZP)); and the Mass Concentration blocks (MASCON) approach with also three processing systems available (JPL-M; CSR-M; Goddard Space Flight Center (GSFC) with GSFC-M).

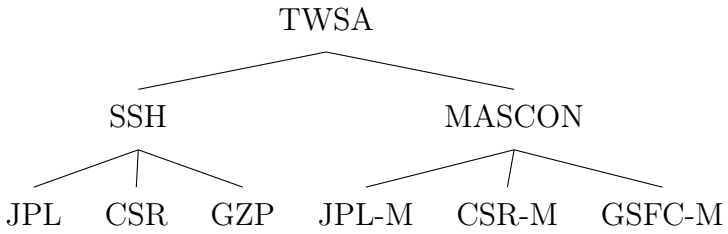

Figure 1: Monthly gravity solutions proposed by GRACE for TWSA calculation (Jing et al., 2019; Chen et al., 2020)

The SSH approach used the first decade of GRACE observations (Landered et al., 2012 ; Swenson, 2012). It suffers from poor solvability in the east-west gradient (Liu et al., 2010), requiring empirical post-processing filtering of the data (Chen et al., 2021). For the treatment of the wavelength signal of the mass variations, main differences between gravity solutions are based on the post-processing step with spatial filtering of the spherical harmonic coefficient (Sakumura et al., 2014). The limitations of SSH smoothing, illustrated by the loss of real geophysical signals, are overcome by the MASCON approach where geophysical constraints are more easily implemented (Watkins et al., 2015). The latest products released (CSR RL06 Mascons solutions) have a resolution of $0.25° * 0.25°$ [3].

The validation of GRACE-based groundwater storage variations can be performed when in situ well measurements are available, following the equation 5 (Thomas et al., 2017 ; Frappart et al.,2018). For the evaluation of groundwater storage variation based on GRACE for the California Central Valley region, Thomas et al. (2017) proposed the Grace Groundwater Drought Index (GGDI) method using the JPL-RL05.1M mascon solution. This method begins with the Groundwater Storage Anomaly (GWSA) calculation. Subsequently, the climatology index for the region is calculated as follows (see equation 9) (Thomas et al., 2014).

[3] $http://www2.csr.utexas.edu/grace/RL06\_mascons.html, 24/05/2021$

$$C_i = \frac{\sum_{i=1}^{n_i}(GWSA_i)}{n_i} \tag{9}$$

where i, the considered month; and n_i = the time period.

At least 30 years should be needed for the calculation of climatology. Yet, the GRACE product is only available since 2002. This limits the potential of this approach. The seasonal influence on groundwater storage is removed by substracting climatology (equation 9) from groundwater storage changes (Jasechko et al., 2014). Thomas et al. (2017) substract climatology from GWSA to get the Groundwater Storage Deviation (GSD) and calculate the GGDI by the equation 10.

$$GGDI = \frac{GSD_t - \overline{x}_{GSD}}{s_{GSD}} \tag{10}$$

with :

- $\overline{x}_{GSD}$: mean of GSD ;
- s_{GSD} : standard deviation of GSD ; and
- GSD_t : GSD function of time.

Thomas et al. (2017) observe a strong relation between GGDI and the in situ GWI (see equation 7), but weak correlation between GGDI and SPI-1. The temporal lag of a drought condition was demonstrated when comparing the groundwater index with SPI-1 five months before the groundwater index is calculated. Guo et al. (2021) also assessed the temporal lag of a drought condition by comparing the SGI with SPI, based on 100 wells with less than 5% of missing data over a period ranging from 1981 to 2010 in four different regions of the United State of America (USA). The best model describing the distribution of SGI was the lognormal distribution function. The comparison, based on the same accumulation period between SPI and SGI, has shown a moderate negative correlation and the lag period didn't change in function of accumulation period for Massachussetts and Washington regions, but increased for Oklahoma and Georgia. This suggests the influence of hydrogeological conditions (vadose zone, lithology, soil, human activity etc.) on groundwater behavior.

2.3 Drought episodes in Tunisia

2.3.1 Historical records

A review of the frequency of drought events based on rainfall deficit during the twentieth century was made by Henia (2003). In this work the annual rainfall data from 1900-1901 to 1989-1990 were used[4]. The rainfall data of each time series have been organized in ascending order and classified in five classes by a cumulative frequency method (see Table 5) :

Classes	cumulative frequency
Very dry	$p(x) < 15\%$
Dry	$15\% < p(x) < 35\%$
Normal	$35\% < p(x) < 65\%$
Humid	$65\% < p(x) < 85\%$
Very Humid	$p(x) > 85\%$

Table 5: Classes retained by the cumulative frequency approach.

In the table 6, "dry" and "Very dry" classes are not distinguished[5]. To evaluate the spatial distribution of drought, the stations are separated in three regions[6]:

- the northern region with Beja and Tunis;
- the central region with Kairouan and Sousse; and
- the southern region with Sfax, Gabès and Gafsa.

For the column SPI-12 and SPEI-12 in table 6, data comes from the Earth2Observe Project funded by the European Union (EU). The data are based on remote sensing and in-situ data [7].The Geographic Information System (GIS) elaborated by this project is called Water Cycle Generator (WCI).It was decided to choose the accumulation period of twelve month in order to maintain the same time resolution with Hénia (2003).
The Tropical Applications of Meteorology using Satellite (TAMSAT) rainfall datasets are used to calculate the SPI. The spatial resolution is $0.0375 * 0.0375$ degree[8] with a temporal resolution of ten days (Fareh et al., 2017).

[4]The year starts on September 1 and ends on August 31.

[5]Droughts from 1900-1901 to 1979-1980 are presented on Table 28 in Appendix

[6]To facilitate the census, when two stations report a drought, a regional drought is considered. When six stations report a drought, a national drought is considered.

[7]*www.earth2observe.eu*, 27/05/21

[8]More or less 4 km^2(www.Tamsat.org.uk, 27/05/21)

Year	(Hénia, 2003)	EMDAT	SPI-12	SPEI-12
1980-1981	Center & South			
1981-1982	Center & South			
1983-1984	Center & South			
1985-1986	North		North & Center	North
1987-1988	Tunisia	Tunisia (1988)	Tunisia (1988)	Tunisia
1988-1989	North			
1989-1990	North			
1993-1994				South (1994)
1994-1995			Center	North & Center(1995)
1995-1996			North	North
1996-1997			Tunisia (1997)	
2000-2001			Tunisia	Tunisia
2001-2002			Tunisia	Tunisia
2007-2008			North & Center	North & Center (2008)
2009-2010			Tunisia (2010)	Tunisia (2010)

Table 6: Drought episode observed from 1980-1981 to 2011-2012

The Global Land Evaporation Amsterdam Model (GLEAM) satellite is used to calculate the actual evapotranspiration for the SPEI. The spatial resolution is 25-50 km with a daily temporal resolution (Fareh et al., 2017).
The timeframe for both datasets goes from 1983 to 2012. Delimited regions and SPI/SPEI evolutions are shown in Appendix. A drought was noted when the value was below -1. The SPI and SPEI show most of the time the same drought episode except for years 1993-1994 and 1996-1997. Spatial differences are observed for years 1985-1986 and 1994-1995.

For the column Emergency Events Database (EMDAT), data comes from the Centre for Research on the Epidemiology of Disasters (CRED) and a disaster is entered into the database when one of the following criteria is fulfilled[9] :

- At least ten people reported killed;
- At least hundred people affected;
- Declaration of a state emergency; or
- Call for an international assistance;

The EMDAT database is mainly based on social impact of drought, which could explain the poor census of drought episodes.

[9] $https://www.emdat.be/explanatory-notes$, 27/05/21

2.3.2 Mapping drought

Due to the difficulties of delimiting the spatial influence of a drought and given that the extent of a drought episode is one of the criteria of its magnitude, geostatistical approaches are needed to be more precise about the geographical impact of a drought. Concerning Tunisia, Gader et al. (2020) studied the variability of precipitations and drought patterns over the Medjerda catchment in north Tunisia. The geostatistical technique used to map this region is the semi-variogram analysis with an ordinary kriging method to predict the annual mean precipitation for unobserved locations, a method already used in Greece by Varouchakis et al. (2018). Results show high spatial variability ranging from 300 mm/year to 1200 mm/year for Medjerda catchment, rainfall amounts gradually decreasing from north to south part of the catchment.

Other statistic approaches, such as L-moment method derived from Probability Weighted Method (PWM) (Greenwood et al.,1979), can also be used for the determination of probability distribution parameters of extreme hydrometeorological variables (Gubareva and Gartsman, 2010). Since the L-moment estimation method use only combination of linear functions of observed datasets, it is less affected by bias in estimation, more robust to outliers and able to characterize more distribution functions than conventional moment methods (Hosking, 1990). This method was implemented accross Tunisia by Sellami et al. (2021) to elaborate a regional drought frequency map with the same procedure than the index flood Regional Frequency Analysis L-Moments (RFA-LM) probabilistic model, which has already shown relevant results for meteorological drought frequency by Núñez et al. (2011) in Chile. The approach structures annual mean precipitation of 62 stations by regions with their own homogeneous probability distribution. Via the quantile estimation of annual precipitation deficit and the return periods of droughts, a spatio-temporal drought map provides valuable features of drought episodes and encouraging tool for drought risk assessments.

3 Materials and methods

In this section, three complementary approaches (an in situ based approach, a model based approach and an approach based on available climatic data) will be implemented to assess drought for the Siliana case study :

First, available generic data on average precipitation will be used to calculate standard meteorological drought indicators, with different lag times.

The piezometric in situ data will provide an observation of the water resources status but only during low and high water season (summer and winter). An indicator will be elaborated to normalize the piezometric datasets. Based on this normalised indicator, drought classes inspired from SPI classes will be arbitrary attributed to specific range of values.

Finally, within the model based approach, a hydrological model will first allow delineating the catchment into subbasins. This spatial redefinition sets the boundaries of the study areas and allows to focus on catchment parts where piezometers are located. The hydrological model will then be used to estimate recharge for those areas of interest and provide a spatio-temporal view of the recharge process. From the recharge datasets, drought classes inspired from SPI classes will also be arbitrary attributed in function of the amount of percolated water.

The three approaches provide different ways to assess drought. A correlation analysis and a confusion matrix analysis will then be be made to compare the 3 different approaches.

3.1 Study site description

3.1.1 Location

Located in the North-West of Tunisia[10], the Siliana catchment drains an area of 1940 km^2 approximately with a mainly mountainous terrain, ranging from 79 to 1299 m (see figure 2). The Siliana river is a tributary of the Medjerda river, the main river in Tunisia with a catchment of aproximately 16400 km^2 on its tunisian part (Mjera, 2015). The cumulated discharge of the Medjerda river represents 37% of average annual input of surface water of the country (Rapport national du secteur de l'eau, 2019).

[10]North latitude : 36°30'.0" 35°50'.0" ; East longitude : 9°0'.00" 9°40'.00"

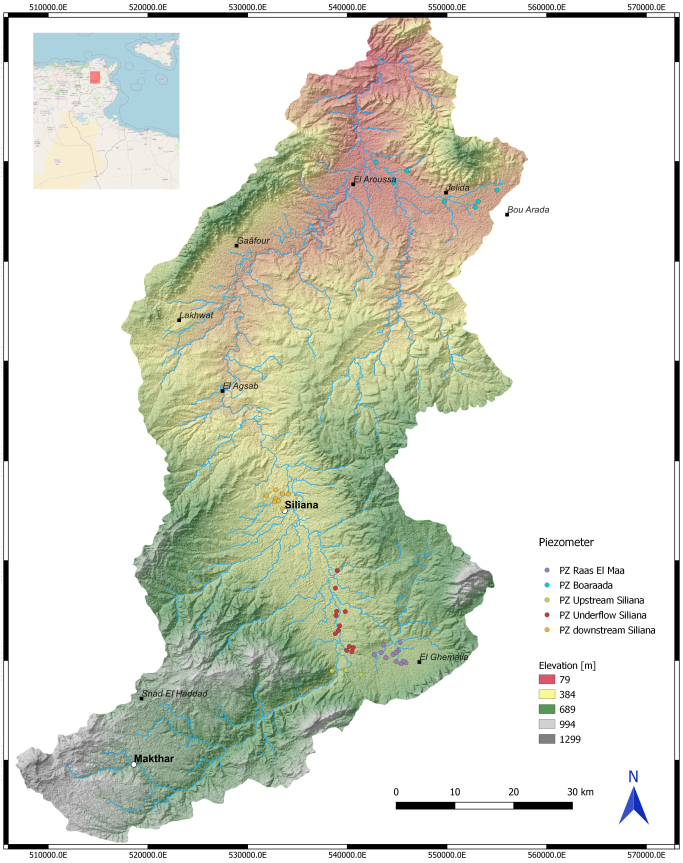

Figure 2: Siliana catchment

3.1.2 Climate

The Siliana governorate is characterized by a mediterranean climate with temperature varying from 3.8C°to 13.3C°for minima and from 18,4C°to 35,3C°for maxima. The average annual rainfall is between 250 to 600 mm.[11] For the Siliana catchment, the average annual rainfall for the period from 1979 to 2009 is 580 mm/y, with december-january being the wettest months and july-august being the driest (El Ghoul, 2017). The catchment situates in the semi-arid bioclimatic zone (Ozenda, 1975; Mjera 2015) and is characterized by a high evaporation potential and a marked risk of water stress. The mountainous topography contributes to

[11] $http://www.environnement.gov.tn/GDTS/index.php?option=com\_content\&view=article\&id=136\&Itemid=787\&lang=fr$, 21/07/2021

high variability in infiltration and Evapotranspiration (ET) dynamics , depending on influence of climatic parameters over southern an northern slopes of moutains (see table 7).

	Temp. (C°)	Insolation (h)	Wind (m/s)	R.H (%)
Winter	10.0	430	3.3	72.1
Spring	15.8	667.3	3.5	68.3
Summer	26.5	945.6	3.4	51.5
Autumn	19.0	587.2	3.2	67.4

Table 7: Seasonal means of climatic parameters for period 2000-2011 on Siliana catchment (INM; Mjera, 2015).

3.1.3 Geology

More than 50% of the geological outcrops are represented by four types of rocks: recent alluvium and marlstone with "yellow balls" (aE2-3), marlstone with calcareous interlayers (cC2), recent alluvium (aQ) and white chalky limestone (dC2) with respectively 19.2, 14, 13.5 and 7.7 percent of the Siliana catchment area (see fig.3 and table 8).

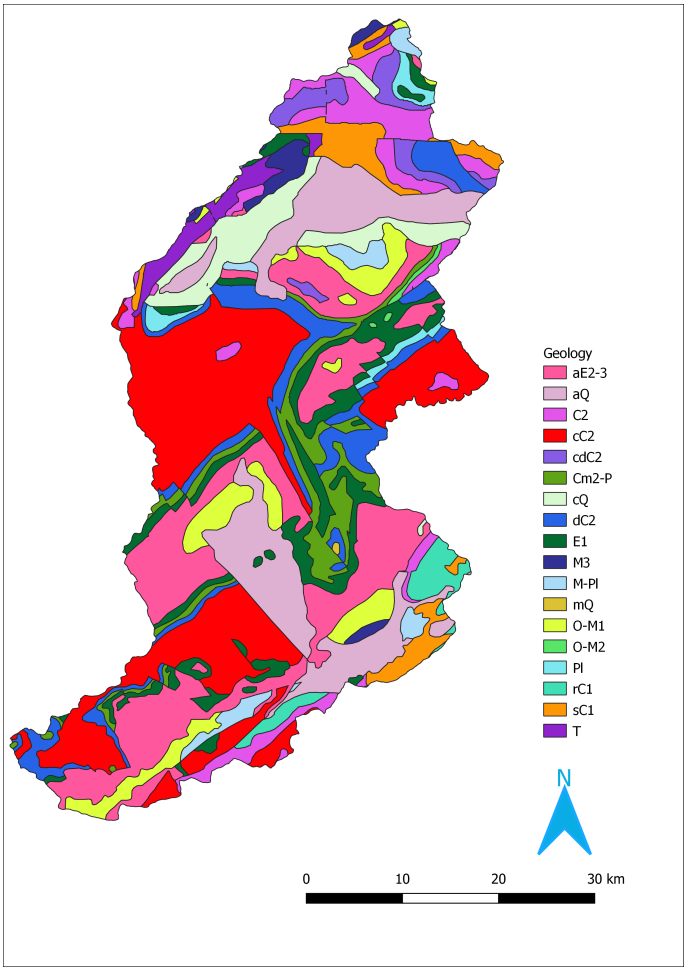

Figure 3: Geology of Siliana catchment (Limbourg, 2021; Carte géologique 1:500.000)

Code	Era	Rock type
	Quaternary	
aQ	Recent and current alluvium	Recent alluvium
cQ	Middle and upper continental pleistocene	Ancient alluviums, calcareous and gyspum
mQ	Middle and upper marine pleistocene (Mainly tyrrhenian)	Coastal beaches and dunes consolidated
	Tertiary	
PI	Marine pliocene	Marlstone and sandstone
M-PI	Miocene - continental pliocene	Conglomerates, sand and clay
O-M1	Aquitanian oligocene	Sandy-clay flyschs
O-M2	Upper oligocene - middle miocene	Marlstone, sandstone and glauconite
M3	Upper miocene	Clay, sandstone and conglomerates
E2-3	Lutetian - priabonian	Marlstones with "yellow balls"
E1	Ypresian	Calcareous with globigerina and flint
Cm2-P	Maastrichtian-paleocene	Marlstone and clay with "yellow balls"
	Secondary	
C2	Unsubdivided upper cretaceous	
cC2	Lower senonian	Marlstone with calcareous interlayers
cdC2	Unsubdivided senonian	
dC2	Upper senonian	White chalky limestone
rC1	Lower cretaceous	Perirecifal limestone
sc1	Lower cretaceous	Marlstone, memo-calcareous and alternating sandstone
T	Trias	Clay, dolomite, sandstone and evaporite

Table 8: Geological codes encountered on the Siliana catchment area (Carte géologique 1:500.000).

3.1.4 Land use

The study area is mainly dedicated to agriculture with a dominant cereals (wheat) production (64% of cultivated area). Other productions are smaller with forest Aleppo pine (11%) and olive groves (7%) (see fig. 4).

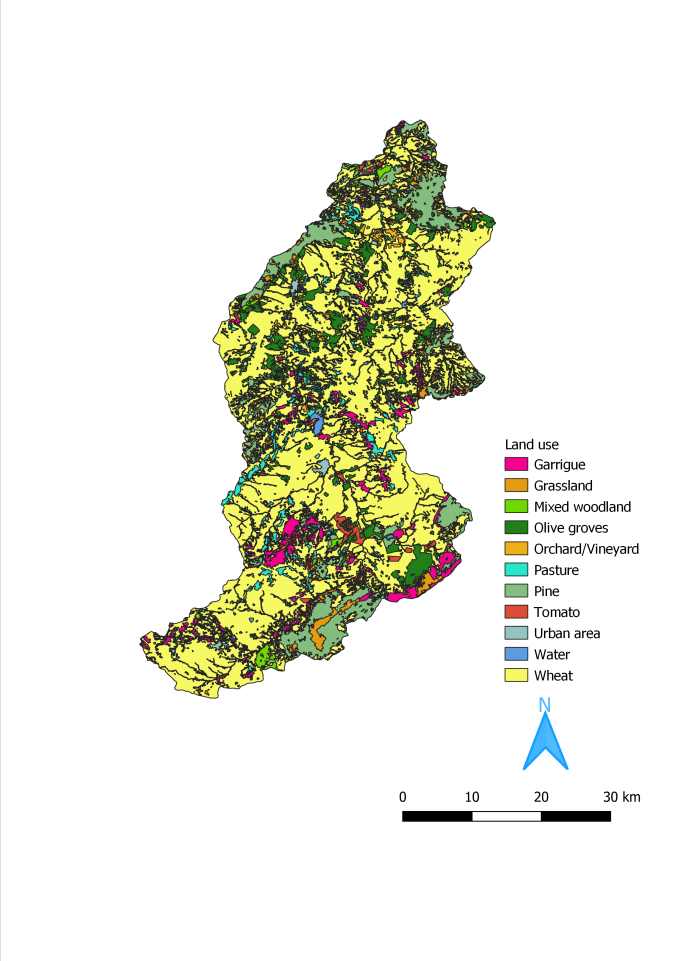

Figure 4: Land use map for Siliana catchment (El Ghoul, 2017)

3.2 The meteorological based drought assessment approach

3.2.1 Calculation of SPI with CHIRPS database

The Climate Hazards group Infrared Precipitation with Stations (CHIRPS) is a quasi-global (50°N-50°S), high resolution (0.05°), daily, pentadal and monthly precipitation dataset (Funk et al., 2015) ranging from 1981 to near present. In

addition to satellite imagery, in situ station data provide gridded rainfall time series for trend analysis and seasonal drought monitoring[12]. The datasets have been retrieved from Google Earth Engine (GEE), a platform which provides a large free catalog of satellite imagery an that can be accessed through the programming language JavaScript and Python.

In order to target the subbasins where the piezometers of the study are located, five shapefiles were extracted from QGIS with sometimes grouped subbasins (see Chapter 3.3).Then, the shapefiles were uploaded on GEE and 1983-2020 precipitation data for each have been downloaded[13] via the written code shown in fig.44 (Appendix). SPI is mathematically based on the cumulative probability of some precipitation recorded at the observation station (Zhang et al., 2017). Guttman (1999) suggests that the Gamma distribution is the most suitable probability distribution to model precipitation data. Hence, a Kolmogorov-Smirnov (K-S) test was applied to the CHIRPS dataset of each subbasin to verify the validity of the Gamma distribution model.

3.2.2 The Kolmogorov-Smirnov test

The K-S test is a non-parametric, goodness of fit statistical test which allows to analyse the type of distribution of a given dataset (Soong, 2004). The test is only valid for continuous distributions. The K-S test measures the deviation of the observed distribution function $F^0(x)$ from the hypothesized distribution function $F_X(x)$. The maximum of this deviation, noted d_2, is calculated via equation 11 :

$$d_2 = max_{i=1}^{n}[|F^0(x_i) - F_X(x_i)|] \quad with \quad i = 1, 2, ...n \tag{11}$$

where x_i are rearranged sample values in increasing order of magnitude and $F^0(x)$ the observed function determined at each (x_i) by the relation $F^0(x_i) = \frac{i}{n}$.

Then a level of significance α is choosen and the maximum absolute value on equation 11 is compared with critical value $c_{n,\alpha}$ shown in fig.45 (Appendix). The null hypothesis of same distribution H_0 is rejected when $d_2 > c_{n,\alpha}$. The python code, written by Creplet (2021) in Spyder software and adapted for the study area, is shown on Fig.46 and 47 (Appendix).

[12] *https : //www.chc.ucsb.edu/data/chirps*, 23/07/2021

[13] Due to large amount of data with daily resolution time, pentad (5 days) resolution time has been downloaded

3.2.3 Gamma probability distribution for SPI

The SPI calculation begins with the Gamma probability density function presented in equation 12 :

$$g(x) = \frac{1}{\beta^{\alpha}\Gamma(\alpha)} x^{\alpha-1} e^{(\frac{-x}{\beta})} \tag{12}$$

where

- $\alpha > 0$: a shape parameter;
- $\beta > 0$: a scale parameter;
- $x > 0$: the precipitation amount; and
- $\Gamma(\alpha)$: the gamma function.

  The Gamma function yields:

$$\Gamma(\alpha) = \int_0^{+\infty} y^{\alpha-1} e^{-y} dy \tag{13}$$

.

For the optimal estimation of α and β parameters, Thom (1966) proposes the following Maximimum Likelihood Estimators (equations 14 and 15) :

$$\hat{\alpha} = \frac{1}{4A}\left(1 + \sqrt{1 + \frac{4A}{3}}\right) \tag{14}$$

$$\hat{\beta} = \frac{\bar{x}}{\hat{\alpha}} \tag{15}$$

with

- $A = \ln(\bar{x}) - \frac{\sum \ln(x)}{n}$;
- n : precipitation observation number; and
- $\bar{x}$: mean of precipitation time series.

The integration of equation 12 provides the expression of cumulative probability presented in equation 16 :

$$G(x) = \int_0^x g(x)dx = \frac{1}{\hat{\beta}^{\hat{\alpha}}\Gamma(\hat{\alpha})} \int_0^x x^{\hat{\alpha}-1} e^{-\frac{x}{\hat{\beta}}} dx \tag{16}$$

As precipitation datasets may contain zeros, the cumulative probability is adapted to consider the censored data (equation 17)

$$H(x) = q + (1 - q)G(x) \tag{17}$$

where

- $q = \frac{m}{n}$ is the probability of no precipitation;
- m : the number of zero in a precipitation dataset; and
- n : number of observations in a precipitation dataset.

To calculate the SPI index, the cumulative probability $H(x)$ must be converted to a standard random variable Z with mean zero and variance of one (Edwards, 1997). This modification, called an equiprobability transformation, is necessary in order to move from a [0,1] distribution, like the Gamma distribution, to a standard normal distribution (Panofsky and Brier, 1958). This transformation is expressed with equation 18 developed by (Abramowitz and Stegun, 1965) :

$$Z = SPI = \begin{cases} -\left(t - \frac{c_0 + c_1 t + c_2 t^2}{1 + d_1 t + d_2 t^2 + d_3 t^3}\right), & 0 < H(x) \leq 0.5 \\ +\left(t - \frac{c_0 + c_1 t + c_2 t^2}{1 + d_1 t + d_2 t^2 + d_3 t^3}\right), & 0.5 < H(x) \leq 1.0 \end{cases} \tag{18}$$

where

$$t = \begin{cases} \sqrt{\ln \frac{1}{(H(x))^2}} & 0 < H\,(x) \leq 0.5 \\ \sqrt{\ln \frac{1}{(1-H(x))^2}}, & 0.5 < H\,(x) \leq 1.0 \end{cases} \tag{19}$$

$d_1 = 1.432788,\ d_2 = 0.189269,\ d_3 = 0.001308$

$c_0 = 2.515517,\ c_1 = 0.802853,\ c_2 = 0.010328$

All thoses steps described for the calculation of SPI have been encoded in the GEE platform by Creplet and Alonso (2021)[14].

3.2.4 Calculation of the $H(x)$ indicator

In order to facilitate the comparison with other drought indicators, the cumulative probability of precipitation $H(x)$ is preferred instead of SPI, because it covers the same bounded range of value [0,1] than the piezometric-based that will be

[14]For the code, please contact marnik.vanclooster@uclouvain.be from UCLouvain Earth and Life Institute (ELI)

presented further. The quantile based approach has been used in many recent drought studies, considering a drought when the value goes below 0.2 (Sheffield et al., 2004; Andreadis et al., 2005; Vidal et al., 2010; Samaniego et al., 2013; Kumar et al., 2015). The correspondence between SPI and $H(x)$ is shown in table[15] 9.

SPI cumulative probability (Z)	Cumulative probability (H(x))
-3	0.0014
-2.5	0.0062
-2	0.0228
-1.5	0.0668
-1	0.1587
-0.5	0.3085
0	0.5
0.5	0.6915
1	0.8413
1.5	0.9332
2	0.9772
2.5	0.9938
3	0.9986

Table 9: Corresponding value of H(x) with SPI (Edwards et al, 1997).

3.3 The drought assessment approach based on in situ piezometric data

3.3.1 Available piezometric data

Fifty four piezometers are reported in the SMART Medjerda project database. Twenty piezometers have been selected as they exhibit data corresponding to the time period of interest (1997-2013) with an acceptable degree of completeness. Those data are shown in the tables 10, 11, 12, 13 and 14 and their locations on Siliana subbasins are presented in fig. 5.

3.3.2 Calculation of indicators

Due to data limitations the simplified Filling Index (FI) and Accumulated Filling Index (AFI), presented in table 4, was used as a basis to calculate an alternative

[15]For the calculation of SPI on GEE, the code is made with inversion of correspondance between H(x) and SPI. So a value above 0.8 is considered as a drought.

	Subbasin(s)	PLmin [m]	PLmax [m]	Start	End	Missing year
Youssef Lab	2,4	12.9	8.03	Apr. 97	Sep. 09	None
U-C-P El Borj	2,4	10.71	4.65	Apr. 97	Sep. 09	None
Boujemaa O.	2,4	5.86	2.45	Apr. 97	Sep. 0.9	None
Puits Djelida	2,4	4.83	0.45	Apr. 97	Sep. 09	None
U-C-P El Mch	2,4	15.36	9.69	Apr. 97	Sep. 09	None
Bir Abdelati	2,4	7.71	2.52	Apr. 97	Sep. 09	06
Ecole Brehga	2,4	14.41	8.25	Apr. 97	Sep. 09	None

Table 10: Piezometers located in the Boaraada groundwater body.

	Subbasin(s)	PLmin [m]	PLmax [m]	Start	End	Missing year
H. Ben Abdelmlek	16	29.1	9.99	Apr. 98	Sep. 13	00/01/02

Table 11: Piezometers located in the Siliana upstream groundwater body.

	Subbasin(s)	PLmin [m]	PLmax [m]	Start	End	Missing year
M'barek ben Med. H.	9	14.45	10	Apr. 97	Sep. 11	00/01/02/04
Salah ben A. Z.	9	19.18	13.52	Apr. 97	Sep. 14	00/01/02/04

Table 12: Piezometers located in the Siliana downstream groundwater body.

groundwater based drought indicator. The drought indicators are referred to as Emptying Index (EI) and Accumulated Emptying Index (AEI) and are defined in equations 20 and 21.

$$EI_i = \frac{PL_i - PL_{max}}{PL_{min} - PL_{max}} \tag{20}$$

	Subbasin(s)	PLmin [m]	PLmax [m]	Start	End	Missing year
Salah Ben Rabeh	17	29.06	17.05	Apr. 97	Apr. 09	00/01
Sassi Ben Med. Taleb	17	18.27	11.56	Apr. 97	Oct. 09	00/01
Amor Ben Ahmed C.	17	32.98	16.15	Apr. 97	Oct. 09	00/01

Table 13: Piezometers located in the Raas El Maa groundwater body.

	Subbasin(s)	PLmin [m]	PLmax [m]	Start	End	Missing year
4343 bis/3	10,14,15,16	33.11	14.36	Apr 97.	Sep. 14	00/01
4450 bis/3	10,14,15,16	48.23	14.35	Apr. 97	Sep. 14	00/01
U2 bis	10,14,15,16	44.94	14.13	Apr. 97	Sep. 14	00/01
P3 BIS	10,14,15,16	37.26	14	Apr. 97	Sep. 14	00/01
Saniet Chraiet	10,14,15,16	33.95	12.35	Apr. 97	Sep. 14	00/01
Romana	10,14,15,16	48.95	22.37	Apr. 97	Sep. 13	00/01
Boukris	10,14,15,16	20.96	12.4	Apr. 97	Sep. 09	00/01

Table 14: Piezometers located in the Siliana underflow groundwater body.

$$AEI = \sum_{i=1}^{m} EI_i \tag{21}$$

EI ranges from 0 to 1, showing respectively the highest water level and the lowest water level observed for a given well. AEI shows the time dynamic of discharge for a given well.

3.3.3 Drought classes based on EI values

From the EI range of values, five classes are arbitrary determined to distinguish drought intensity (table 15).

Classes	EI [-]
Very humid	0-0.15
Humid	0.15-0.35
Normal	0.35-0.65
Dry	0.65-0.85
Very dry	0.85-1

Table 15: Classes retained for EI.

3.4 Drought assessment based on hydrological modelling

3.4.1 Description of the model and data available

The Soil and Water Assessment Tool (SWAT) model is a physically based hydrological model elaborated in order to predict impact of soil management on water, sediments and agricultural chemical yields in ungaged basins. With the use of readily available inputs, long period simulations are possible without calibration (Arnold et al., 1998). Physically based models are mathematical idealization of real phenomenon, with parameters depending on time and characteristics of the study area (Devia et al., 2015). The water balance calculated by SWAT is presented in equation 22 :

$$SW_t = SW_0 + \sum_{i=1}^{t}(R_v - Q_s - ET - W_{seep} - Q_{gw}) \tag{22}$$

with :

- SW_t : Soil water content at time t [mm];
- SW_0 : Soil water content at time 0 [mm];
- R_v : Rainfall volume during the time increment [mm];
- Q_s : Surface runoff during the time increment [mm];
- ET : Evapotranspiration during the time increment [mm];
- W_{seep} : Infiltration from soil to underlying layers during the time increment [mm];
- Q_{gw} : Groundwater runoff during time increment [mm]; and
- t : Time [days].

The infiltration model proposed by SWAT+ for daily rainfall inputs is based on the Curve Number method (USDA-NRCS, 2004). This empirical model calculates surface runoff and subsurface flow by integrating land use, soil type and humidity. The PET is calculated via the Penman-Monteith method (Neitsch et al., 2005). All data available are shown in table 16.

Data	Resolution	Source
Precipitation	Daily (1979-2009)	7 stations (DGRE Tunisia)
Temperature	Daily (1979-2009)	9 climatic stations (SWAT generated 22 Km grid)
Wind/Solar radiation/ Humidity	Daily (1979-2009)	9 climatic stations (SWAT generated 22 Km grid)
DEM	30 m	SRTM
Soil data	1 : 50 000	Agricultural map ; Soil database (Sellami et al., 2014)
Landuse	1 : 5000	Agricultural map (Khlifi, Projet WBI) Landuse database (SWAT model crop database)
Flow rate	Daily (09/1975-08/2008)	DGRE (Tunisia)

Table 16: Input data for SWAT+ model (El Ghoul, 2017).

The model has already been used in Tunisia, showing good performance to simulate flow rates, erosion and sediment behaviour (Aouissi et al., 2014; Ouessar et al., 2009; Sellami et al., 2016; El Ghoul, 2017).

The data used for this section have been made available by El Ghoul (2017) who implemented previously the SWAT model in the ARC-SWAT version of the model. In this section the implementation of SWAT+ within the QGIS environment is explained.

3.4.2 Watershed delineation and soil/land use databases integration

The first step in setting up the hydrological model constists in the delineation of the Siliana catchment and the watershed network. Use is made of the Digital Elevation Model (DEM) provided by the Shuttle Radar Topography Mission (SRTM).This step separates the watershed into 19 subbasins, presented on fig. 5.

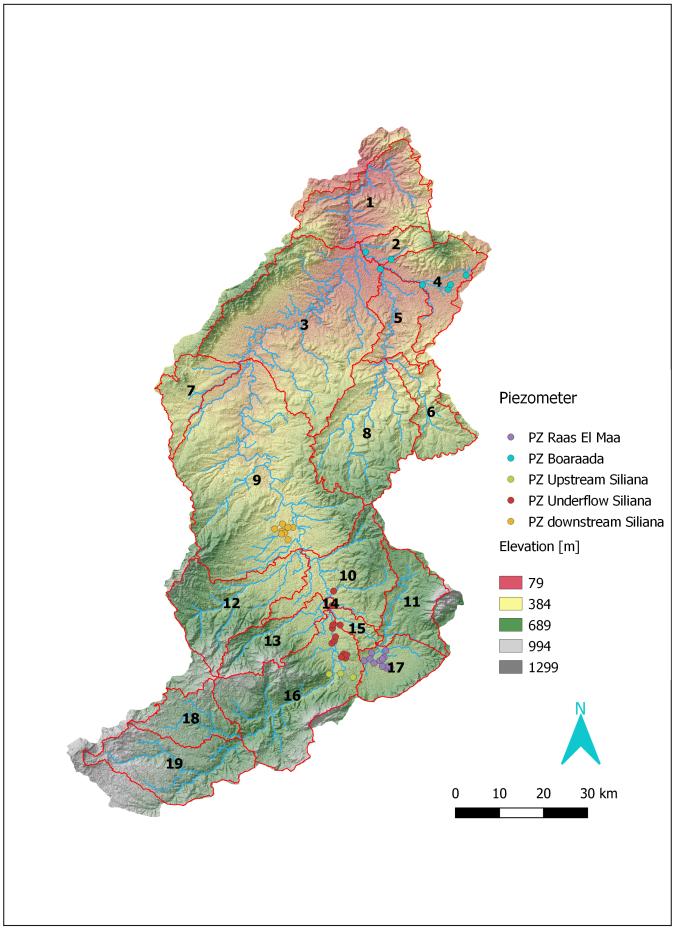

Figure 5: Siliana subbasins generated by the watershed delineation.

After the delineation of the geometrical properties of the catchment, land use and soil databases are integrated in the model. The tunisian soil characteristics were provided by Sellami et al. (2014) and added to the SWAT database. The following parameters were integrated: soil depth, water holding capacity, soil profile, grain size etc. Eleven soil types and fifteen land use classes were identified for the region (see table 17). The catchment has been separated into two classes of slopes, lower and higher than 5 %. The soil and land use feature of the differ-

Soil code	Soil type[16]	Land use code	Land use type[17]
S-700	Lithosol/Regosol	WWHT	Wheat
S-701	Undeveloped soil	GRAR	Row crops
S-702	Rendzina	PINE	Pine tree
S-703	Brown calcareous soil	BARR	Barren
S-705	Vertisol	FRST	Forest
S-706	Isohumic soil	OAK	Oak tree
S-708	Fersiallitic soil	OLIV	Olive groves
S-709	Halomorphic soil	ORCD	Orchard/Vineyard
S-711	Complex soil	PAST	Pasture
S-712	Urban Area	RANG	Range grasses
S-714	Wadi	TOMA	Tomato
		URHD	Urban high density
		URML	Urban medium-low density
		URMD	Urban medium density
		WATR	Water

Table 17: Soil and land use types for the Siliana catchment.

ent subbasins are presented in table 18. Wheat production is dominant in every subbasin, excepted for the second one where pine forest is the dominant land use.

Subbasin	Area [km^2]	Mean elevation [m]	Slope < 5% (%)	Dominant soil texture (%)	Dominant land use (%)
1	122.53	238.53	17.91	S-711 (35.92)	WWHT (46.80)
2	25.72	310.53	18.51	S-711 (45.65)	PINE (39.71)
3	293.88	327.35	26.57	S-703 (28.04)	WWHT (64.68)
4	69.33	315.69	26.12	S-703 (46.74)	WWHT (75.77)
5	56.81	250.76	30.95	S-703 (37.31)	WWHT (82.67)
6	56.73	449.05	18.31	S-703 (29.98)	WWHT (57.07)
7	50.68	405.32	27.22	S-702 (39.54)	WWHT (78.92)
8	147.64	488.72	17.83	S-711 (39.55)	WWHT (73.53)
9	363.87	444.77	26.44	S-703 (33.18)	WWHT (69.24)
10	100.29	564.17	24.61	S-705 (22.31)	WWHT (77.34)
11	65.74	673.35	22.67	S-711 (36.81)	WWHT (70.72)
12	118.04	634.32	20.63	S-700 (27.74)	WWHT (73.50)
13	59.55	675.45	19.96	S-711 (43.69)	WWHT (49.28)
14	1.38	446.01	46.19	S-701 (98.76)	WWHT (80.63)
15	15.21	505.30	29.91	S-703 (37.50)	WWHT (39.24)
16	175.34	707.82	18.28	S-700 (29.23)	WWHT (47.34)
17	54.17	607.17	29.99	S-711 (46.31)	WWHT (30.79)
18	54.75	815.55	28.33	S-703 (35.73)	WWHT (84.57)
19	109.46	865.75	19.49	S-701 (26.04)	WWHT (69.22)

Table 18: Physical attributes of the Siliana subbasins.

3.4.3 Creating HRU

SWAT+ is a semi-distributed model which, in addition to a spatial division into subbasins, proposes a division into Hydrological Response Unit (HRU). Spatial discretization into HRU's is determined by the slope class, soil type and land use. The HRU allows representing the spatial heterogeneity of the study area. The number of HRU's is manually selected in SWAT+. In order to avoid too long calculation processes, 279 HRU's have been calculated for the model. Then the HRU with largest area of each subbasin has been considered as representative of the considered subbasin.

3.4.4 Climatic datasets integration and simulation

The last step concerns the addition of climatic data. Data for seven stations[18] located on the catchment were available for precipitation (see table 16). Other climatic data such as temperature, wind, solar radiation and humidty comes from 9 climatic locations available in SWAT database[19]. The model was implemented using a monthly time step from 1997 to 2013. A warming-up period of 3 years was considered, which means that the modelling output is only considered from 2000 to 2013. The time dynamics can be directly observed within the QGIS interface. No calibration was done in this study, because the software SWATCUP+ wasn't freely available. Nonetheless, the SWAT software has been elaborated with the aim of predicting hydrological behaviour with a minimum effort of model calibration (Arnold et al., 1998).

3.4.5 Calculation of recharge based drought indicator

From the model, monthly percolation data are retrieved for each subbasin where piezometers are located, by selecting HRU's where percolation occurs. This indicator, called Percolation Drought Index (PDI), is only based on classes related to recharge amount ranges and presented on table 19.

Classes	PDI [mm]
Very humid	> 50
Humid	30-50
Normal	15-30
Dry	5-15
Very dry	0-5

Table 19: Classes retained for PDI.

[18] Bargou, Bousalem, Bouarada, Bargou, Makthar, Touboursouk, Siliana
[19] *http : //swat.tamu.edu/*

3.5 Correlation between H(x) and EI

The correlation between H(x) and EI is calculated to analyse the consistency between the meteorological drought and hydrogeological drought assessment. The correlation code has been written in a Jupyter Notebook software with Python language and it is available in appendix (Fig.48, 49, 50 and 51). An example of plot for the evolution of EI for Youssef Lab piezometer and the H(x)-9 for the subbasins 2 and 4 is presented in fig.6. The test used is the Spearman's rank correlation test

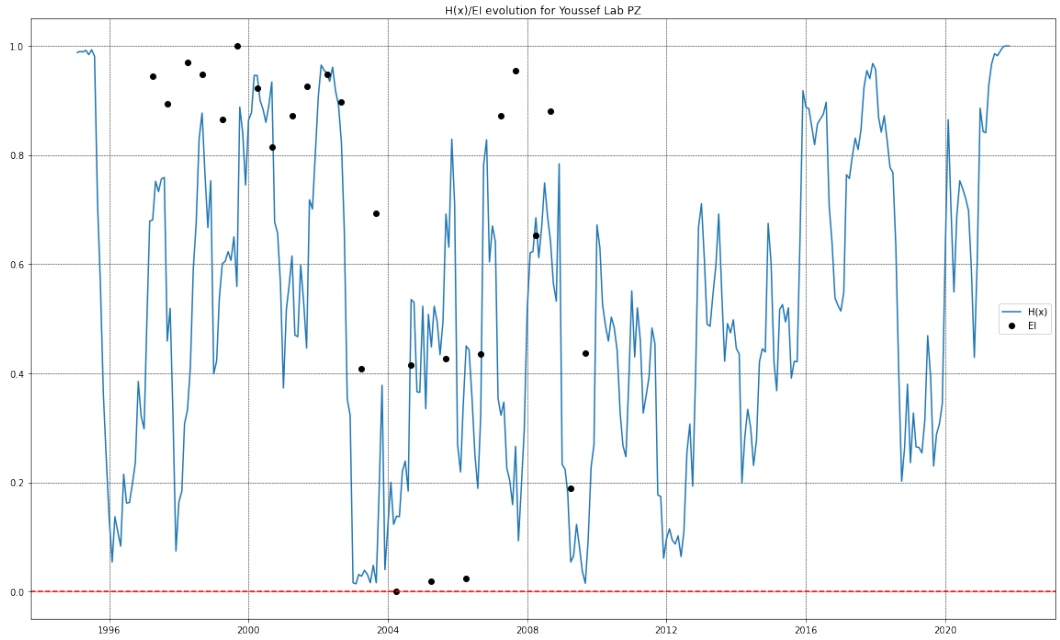

Figure 6: Evolution of EI and H(x)-9 for the Youssef lab piezometer.

The Spearman's rank correlation coefficient presented in equation 23 is a robust non-parametric test elaborated by Spearman (1904) which evaluates the statistical dependence between the ranks of two observed variables instead of their actual values, as it is the case with the Pearson correlation (Croux and Dehon, 2010). This test assesses to what extent a monotonic function can describe the relation between two variables. The monotonic should not be a linear function, and the distribtion of the variables should not be a normal distribution :

$$\rho = 1 - \frac{6 \sum d_i^2}{n(n^2 - 1)} \tag{23}$$

where

- d : the pairwise distances of the ranks of the variables xi and yi; and
- n : the number of samples.

The non-linearity and the non-normal distribution are observed in fig. 7 for the Abdelmlek piezometer and H(x)-6 for the subbasin 16. For other subbasins, non-linearity and non normal distribution are observable in appendix (fig. 52 ,53 ,54 and 55).

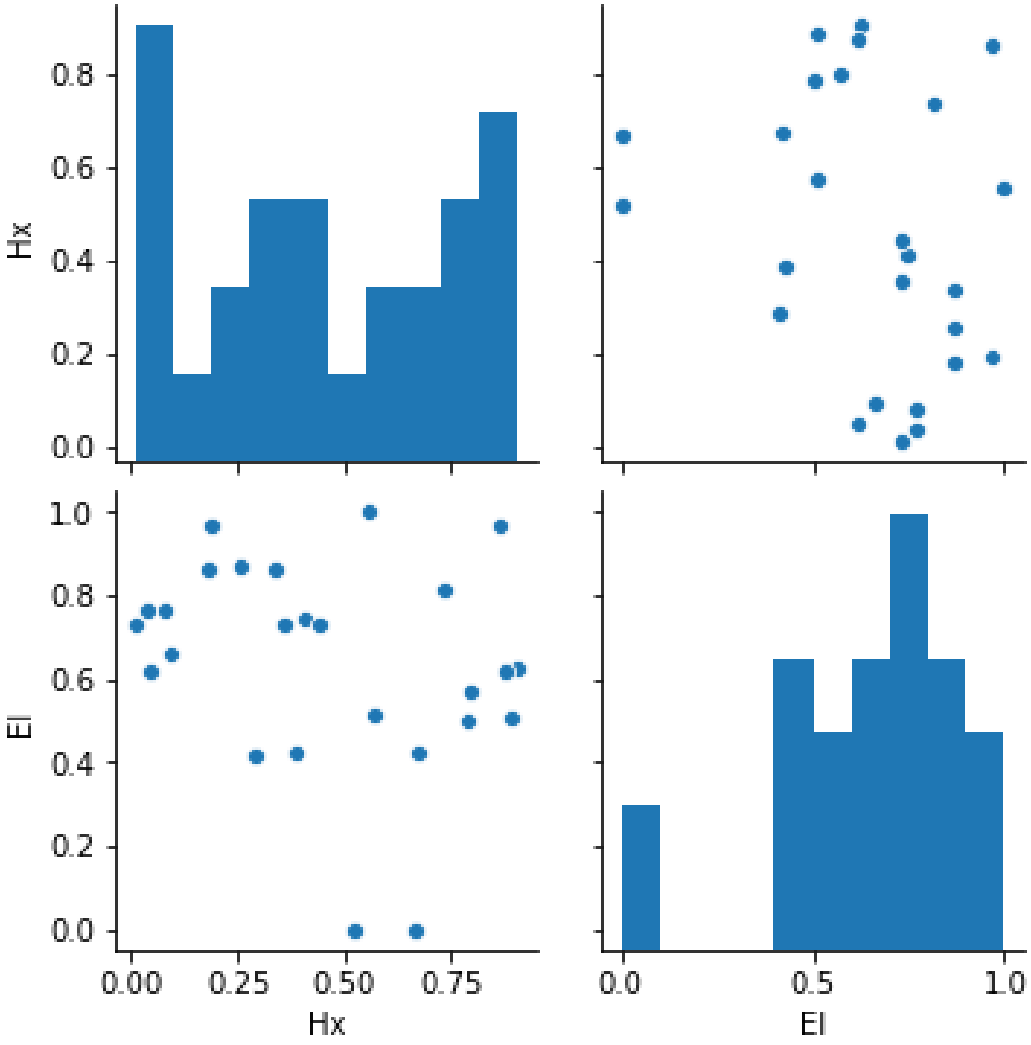

Figure 7: Distribution of EI and H(x)-6 for the Abdelmlek piezometer.

The interpretation of the correlation coefficient score is explained in table 20.

Coefficient interval	Correlation strength
.000-.199	Very weak
.200-.399	Weak
.400-.599	Medium
.600-.799	Strong
.800-.999	Very strong

Table 20: Interpretation of coefficient correlation.

3.6 Confusion matrix between H(x), PDI and EI

The five classes proposed for EI and PDI in tables 15 and 19 are compared with existing classes for H(x). The "extremely dry" and "extremely wet" classes from table 3 are included in "Very dry" class to make the comparison easier. This comparison aims to validate the potential reliability of proposed classes for EI and PDI. Then EI and PDI classes will also be compared together. Confusion matrices and their accuracy are implemented on Jupyter Notebook with the sci-kit Python library.

4 Results and discussions

Results and discussions will be subdivided according to groundwater bodies.

Spearman's correlation tables compare EI of each piezometer with H(x) for different accumulation periods (see tables 23, 24, 25, 26 and 27). Accumulation periods range from one to 24 months and aim to identify which accumulation period best links meteorological and hydrogeological drought for each groundwater body.

Then, the evolution PDI in subbasins where groundwaters bodies are located is compared with H(x) 9, 8, 26 and 27. The use of H(x))-24 is used for these groundwater bodies where many piezometers are available, based on the observed coefficient of correlation in tables 23 and 27. For other groundwater bodies where small number of piezometers are availablee, H(x)-12 is used. This is consistent with recommandations to assess intermediate-term droughts (Edwards, 1997). Both indicators are further compared with EI evaluated for all piezometers located within the respective groundwater body.

Finally, confusion matrices between H(x)-12 or H(x)-24 (depending on groundwater body) and PDI are made. Predicted drought classes for EI are also compared with H(x) and PDI drought classes for some piezometers selected on each groundwater body. The accuracy of the confusion matrices is presented in table 21 and 22.

Subbasins	Accuracy
2,4	0.01
16	0.02
9	0.05
17	0.02
10,14,15,16	0.05

Table 21: Accuracy of each confusion matrix between PDI and H(x) for different subbasins in the Siliana catchment.

Piezometer	PDI	H(x)
Boujemaa	0.10	0.28
El Borj	0.26	0.24
Ecole Bregha	0.20	0.15
Youssef Lab	0.40	0.23
Hammadi Ben A.	0.23	0.35
Salah Ben Abdelafidh Z.	0.12	0.12
Mbarek Ben Med H.	0.38	0.11
Amor Ben Ahmed C.	0.37	0.16
Sassi Ben Med. Taleb	0.37	0.12
PZ P3 bis	0.08	0.39
PZ 4343 bis/3	0.00	0.39
PZ 4450 bis/3	0.12	0.19
Romana	0.12	0.35

Table 22: Accuracy for each confusion matrix of EI classes with PDI and H(x) classes.

4.1 Boaraada groundwater body

	H(x)-1	H(x)-3	H(x)-6	H(x)-9	H(x)-12	H(x)-18	H(x)-24
Youssef Lab	0.088	0.255	0.451	0.387	0.460	0.517	0.529
U-C-P El Borj	0.159	0.402	0.436	0.454	0.499	0.535	0.487
Boujemaa O.	-0.176	-0.023	0.193	0.343	0.274	0.397	0.454
Puits Djelida	-0.097	0.011	0.274	0.504	0.481	0.563	0.580
U-C-P El Mch	-0.139	-0.083	0.025	0.192	0.241	0.271	0.293
Bir Abdelati	0.018	0.125	0.253	0.406	0.429	0.480	0.550
Ecole Brehga	-0.111	-0.010	0.221	0.450	0.478	0.503	0.549

Table 23: Spearman's rank correlation coefficient between EI and H(x) for Boaraada groundwater.

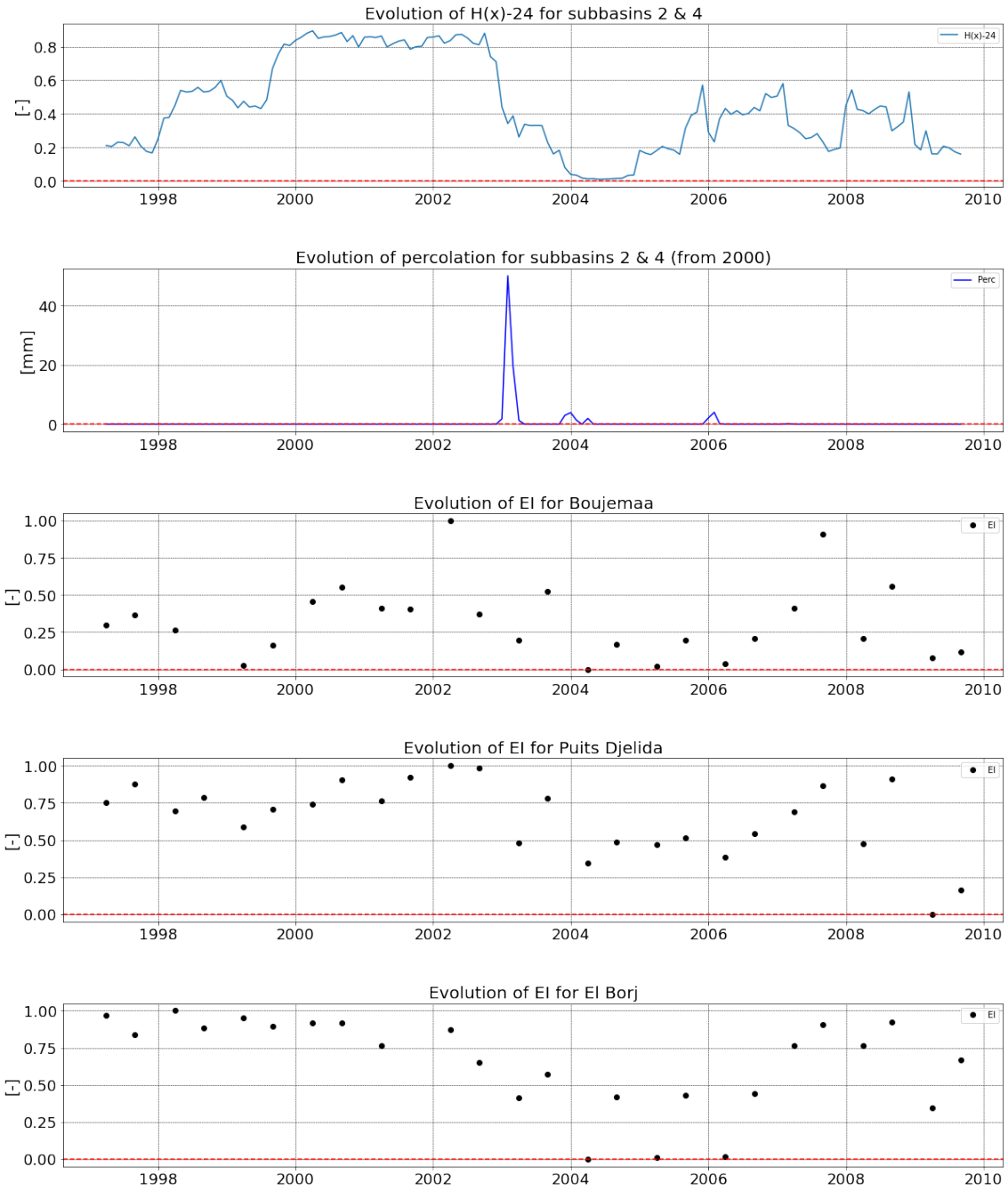

Figure 8: Evolution of H(x)-24, percolation and EI index for piezometers located at Boaraada groundwater body (1/2).

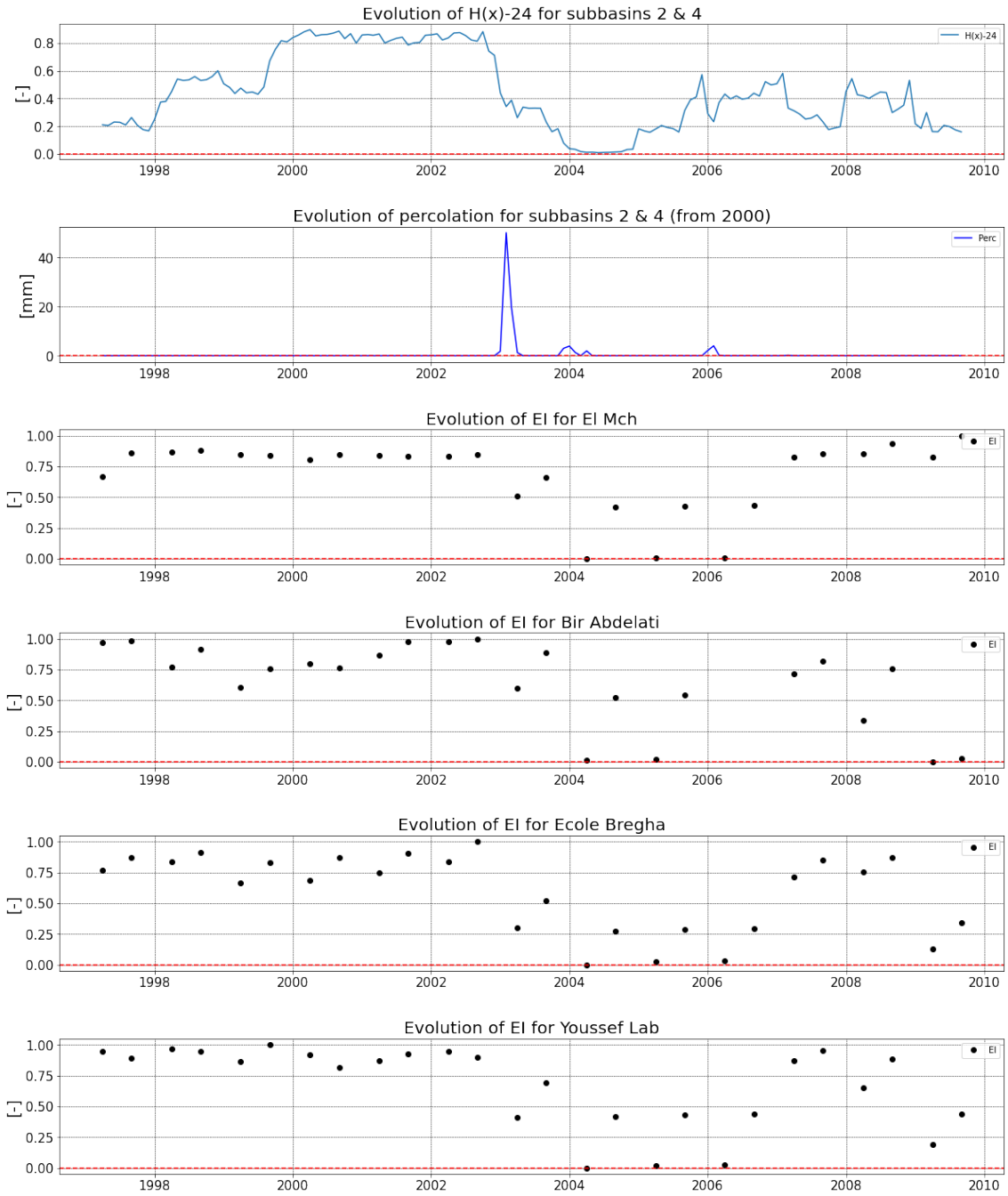

Figure 9: Evolution of H(x)-24, percolation and EI index for piezometers located at Boaraada groundwater body (2/2).

The Boaraada piezometers are scattered on subbasins two and four. The land use of this groundwater body is characterised by a majority of pine tree and wheat

crops. The soils are complex soils over the subbasin two and brown calcareous soils over the subbasin four. Most piezometers show that drought is important (fig. 8 and 9) with a quite regular high level for EI from 1997 till 2003. The "Boujemaa O." piezometer, however, behaves anomalous in this water body. This piezeometer exhibits a low value for the hydrogeological drought indicator for the complete observed period. The change in the water level in the wells coincides with the important recharge episode observed with SWAT+ in 2003. This recharge ended the long drought that affected the whole country from 2000 to 2002. The 2004 and 2006 recharge coincide with expected winter recharge and can be observed in the dynamic of all piezometers. From 2007 onwards, a rise in the pressure on water resources is observed. Indeed, 2007 was a year characterised by a drought located in the north and the center of Tunisia, as confirmed by the evaluation of SPI-12 and SPEI-12 (table 6). Yet this was not assessed by the H(x)-24, showing a value near from 0.5 and corresponding to a near normal situation following tables 3 and 9.

The Spearman's rank correlations between H(x) and EI (table 23) increase for most piezometers in terms of the lag time of H(x), except for "U-C-P El Borj" piezometer. For this last piezometer the maximum correlation is obtained for H(x)-18. The coefficients show all medium correlation except for except for "U-C-P El Mch" piezometer with $\rho = 0.293$. The best value is attained by "Puits Djelida" with $\rho = 0.580$. This difference between rank correlation values can be explained by the depth of well. Indeed, the "U-C-P El Mch" shows the deepest record for piezometric levels (15.35 m) and "Puits Djelida" the shallowest (4.83 m). This logic is in accordance with the theoretical expectation about relationship between accumulation period and depth of water table reported by Li and Rodell (2015) and observed by Kumar (2016).

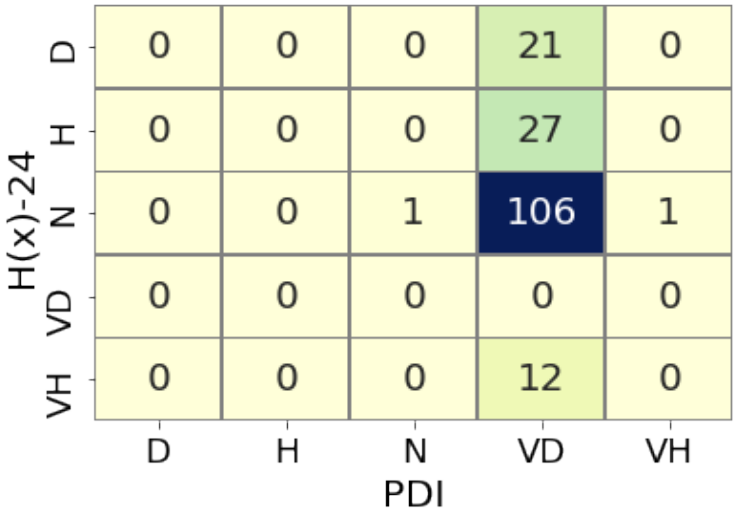

Figure 10: Confusion matrix between H(x)-24 and PDI for subbasins 2 and 4.

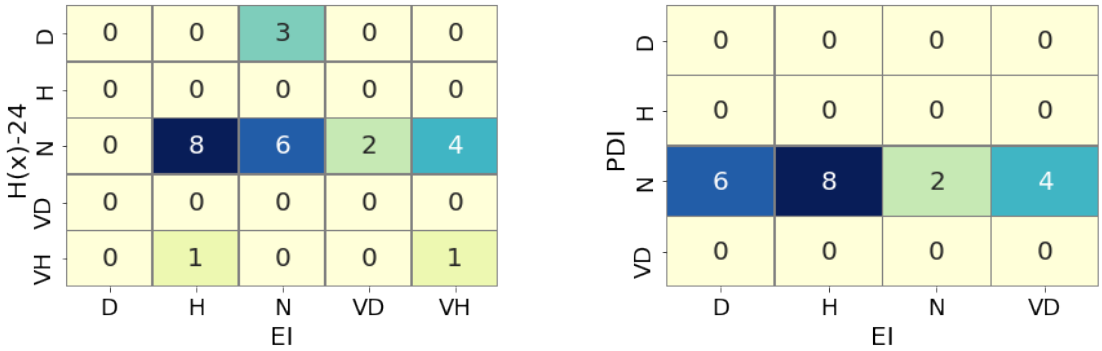

Figure 11: Left : Confusion matrix between EI and H(x)-24 for Boujemaa piezometer. Right : Confusion matrix between EI and PDI for Boujemaa piezometer.

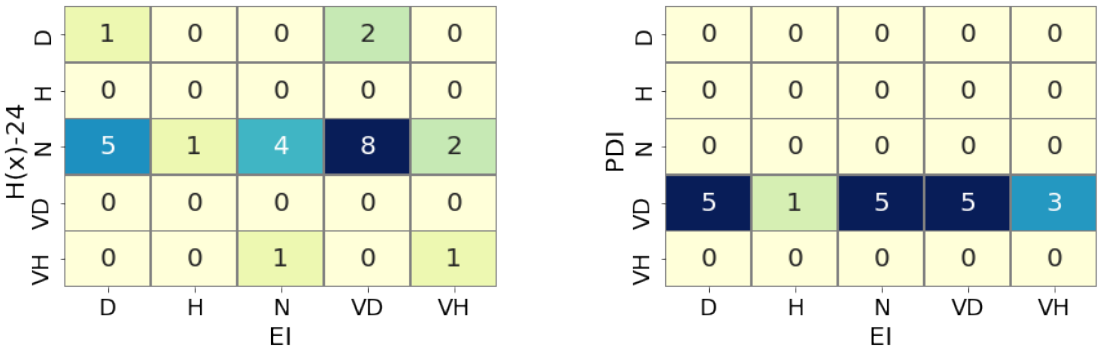

Figure 12: Left : Confusion matrix between EI and H(x)-24 for El Borj piezometer. Right : Confusion matrix between EI and PDI for El Borj piezometer.

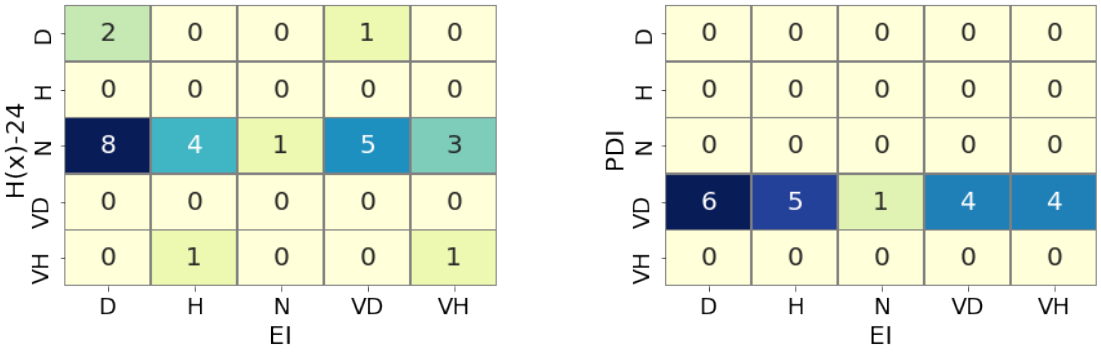

Figure 13: Left : Confusion matrix between EI and H(x)-24 for Ecole Bregha piezometer. Right : Confusion matrix between EI and PDI for Ecole Bregha piezometer.

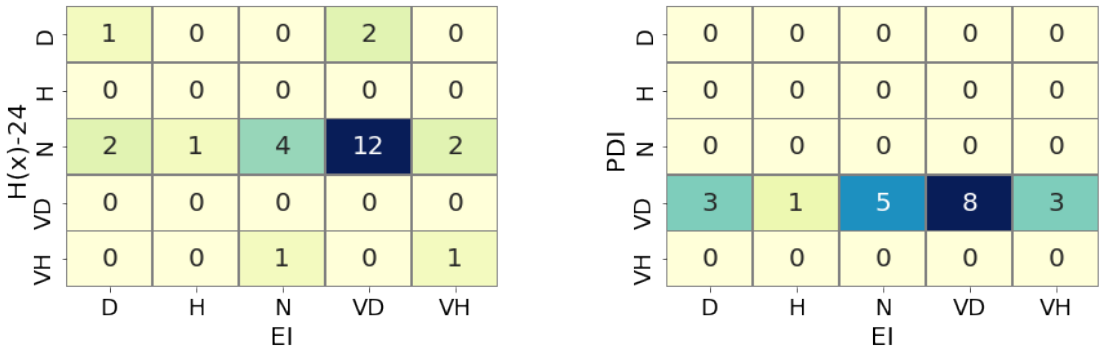

Figure 14: Left : Confusion matrix between EI and H(x)-24 for Youssef Lab piezometer. Right : Confusion matrix between EI and PDI for Youssef Lab piezometer.

Concerning the confusion matrices, PDI predicted classes and H(x)-24 true classes exhibit a poor accuracy (table21) with a value close to zero. In contrats, EI shows better consistency. The largest consistencies between EI and PDI or $H(x)$ is attained for the Youssef Lab, with an accuracy of 0.40 and for Boujemaa for EI-H(x)-24 with an accuracy of 0.28. For piezometers, "Normal" class is the most correctly identified for EI-H(x) and "Very dry" for EI-PDI. Nonetheless, number of misclassifications is much higher. Those values are too weak, suggesting a bad drought classification method for PDI and EI classes. Furthermore, "Very dry" class is predominant in PDI, where all zero values belong to this class which biases the calculation of the values in the confusion matrix.

4.2 Siliana upstream groundwater body

	H(x)-1	H(x)-3	H(x)-6	H(x)-9	H(x)-12	H(x)-18	H(x)-24
Hammadi Ben A.	-0.265	-0.325	-0.301	-0.210	-0.155	-0.085	0.044

Table 24: Spearman's rank correlation coefficient between EI and H(x) for Siliana upstream groundwater.

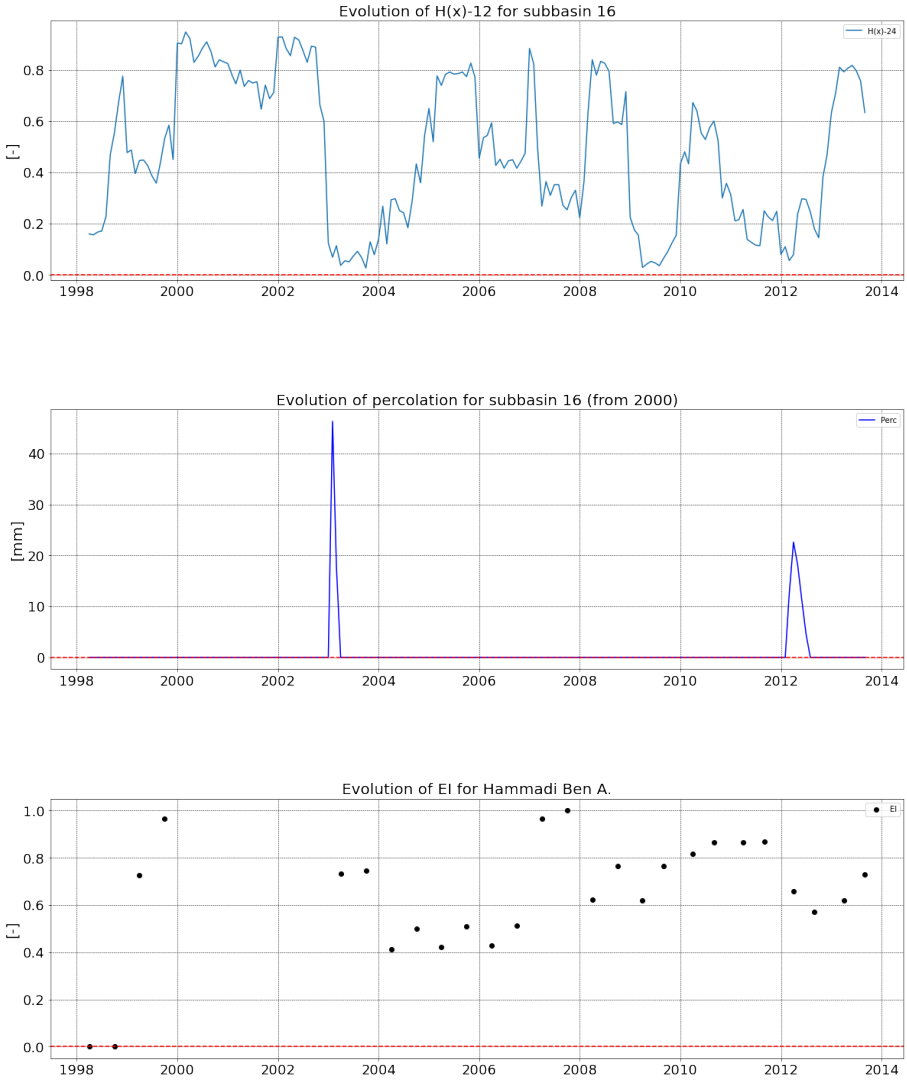

Figure 15: Evolution of H(x)-12, percolation and EI index for piezometer located at Siliana upstream groundwater body.

The Siliana upstream piezometers are located on subbasin sixteen, caracterised by a dominance of wheat crops and lithosols/regosols. Missing data for 2000-2002 period limit the interpretation (fig. 15). A moderate to high drought pressure is observed at the beginning of 2003, which shows possible consequences of 2000-2002 drought. This is followed by an important recharge at the beginning of 2004. The discharge following the drought of 2007 is clearly marked. The consequences of drought of 2010 seems to be persistant until 2012. In 2012 a long recharge period occurred which coincides with low values of H(x)-12.

The Spearman's rank correlation (table 24) shows for this groundwater body that the best coefficient ($\rho = -0.325$) is obtained with H(x)-3. Yet, we should expect a higher coefficient at longer accumulated period for H(x) (Edwards, 1997) especially as the well is rather deep with 29,1 m for the deepest level recorded (Li and Rodell, 2015). The result was not taken into consideration because of the few wells available. The H(x)-12 has been selected for calculating the confusion matrices.

Confusion matrices show near zero accuracy for H(x)-PDI classes (a = 0.02) and weak accuracy for EI-H(x) (a = 0.35) and EI-PDI (a = 0.23) classes, observable respectively in figures 16 and 21. The normal class is the most coinciding for EI-H(x) and the very dry class for EI-PDI. "Normal" class is the best identified for piezometer indicators.

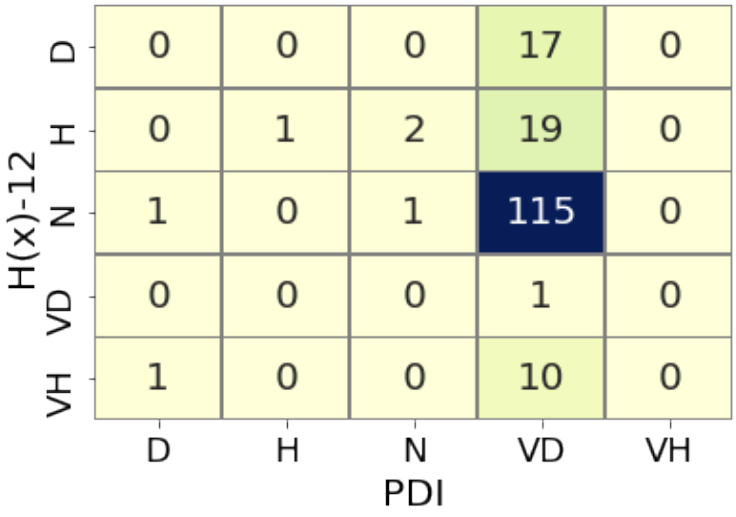

Figure 16: Confusion matrix between H(x)-12 and PDI for subbasin 16.

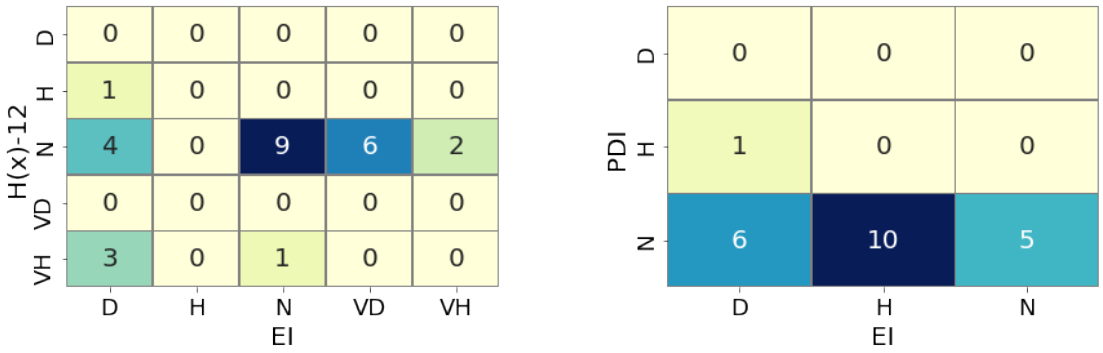

Figure 17: Left : Confusion matrix between EI and H(x)-12 for Hammadi Ben A. piezometer. Right : Confusion matrix between EI and PDI for Hammadi Ben A. piezometer.

4.3 Siliana downstream groundwater body

	H(x)-1	H(x)-3	H(x)-6	H(x)-9	H(x)-12	H(x)-18	H(x)-24
M'barek ben Med. H.	0.338	0.443	0.517	0.523	0.477	0.461	0.258
Salah Ben Abdelafidh Z.	0.093	0.111	0.100	0.405	0.413	0.382	0.415

Table 25: Spearman's rank correlation coefficient between EI and H(x) for Siliana downstream groundwater.

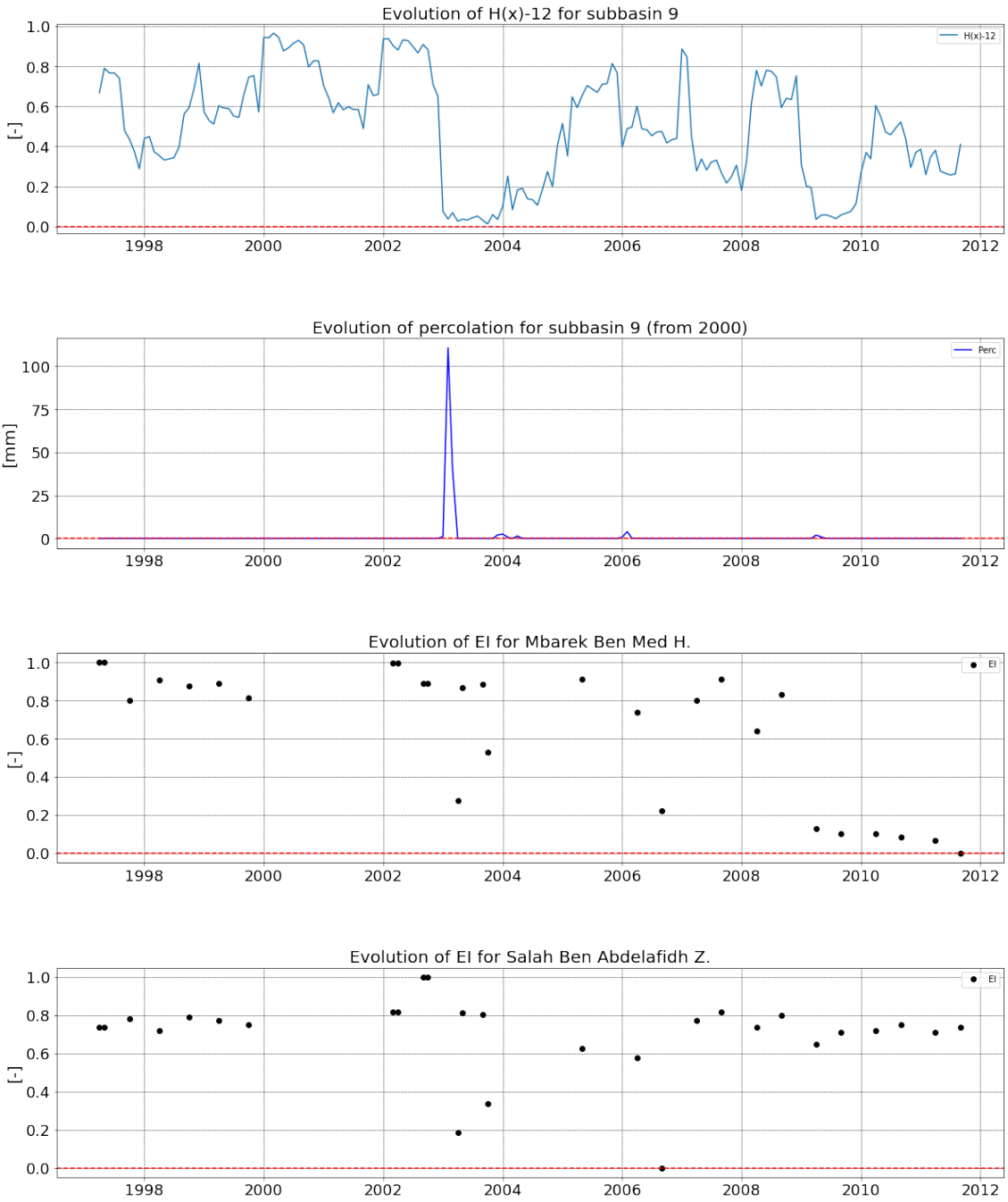

Figure 18: Evolution of H(x)-12, percolation and EI index for piezometers located at Siliana downstream groundwater body.

The Siliana downstream piezometers are located in subbasin 9, characterised by a dominance of wheat crops and brown calcareous soils. These piezometers (Fig.18)

have quite a lot of missing data (2000-2002, 2004) and the available records begin with a middle/high pressure on water resources, that could be initiated with the 1997 drougth. The possible consequences of the 2000-2002 drought and the recharge of 2003 is observable.

For the "M'barek ben Med. H." case, the drought of 2007 is remarkable with an EI passing from 0.25 at the end of 2006 to 0.80 and above in 2007. Then after 2009 the pressure on water resources is low until the end of records in 2011. In this place the 2010 drought is not observable. The best coefficient correlation is observed for H(x)-9 ($\rho = 0.523$) (see table 25).

Concerning "Salah ben A.Z.", the drought of 2007 matchs with the rising of EI from 0 to 0.80. Then a constant normal pressure on water resources is observable with a value above 0.5 for EI until the end of the records in 2014[20]. The best correlation coefficient is observed for H(x)-24 ($\rho = 0.415$). The asymmetry in records length could partly explain the important differences between the Spearman's rank results. Indeed, the M'barek ben Med. H. observations stop in september 2011, while the Salah ben A.Z. observation stop in september 2014 (table 12 in chapter 3).

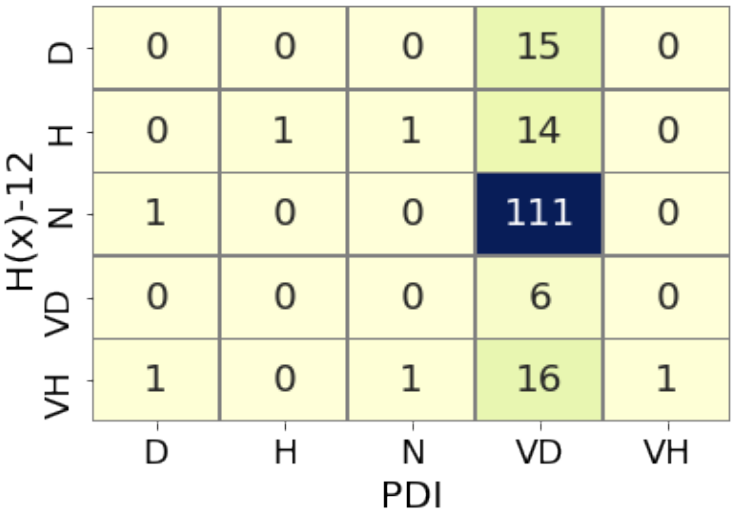

Figure 19: Confusion matrix between H(x)-12 and PDI for subbasin 9.

[20]For the good readability of the graphs, the temporal scale was limited in 2012 coinciding with the well with the shortest time record

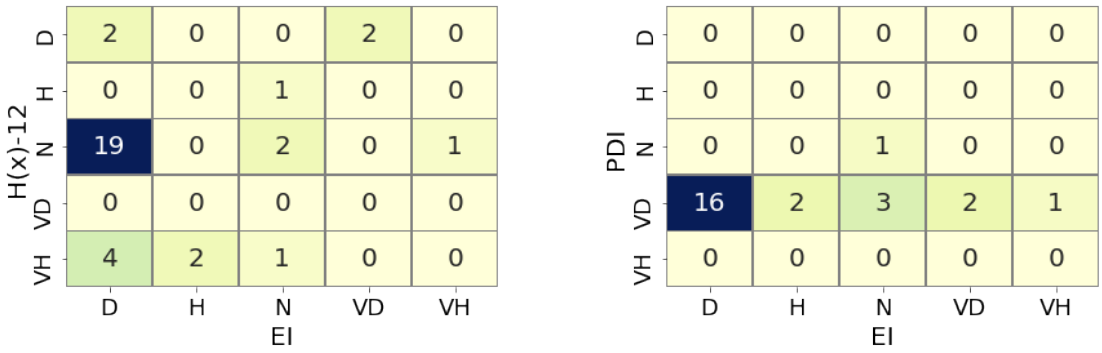

Figure 20: Left : Confusion matrix between EI and H(x)-12 for Salah Ben Abdelafidh Z. piezometer. Right : Confusion matrix between EI and PDI for Salah Ben Abdelafidh Z. piezometer.

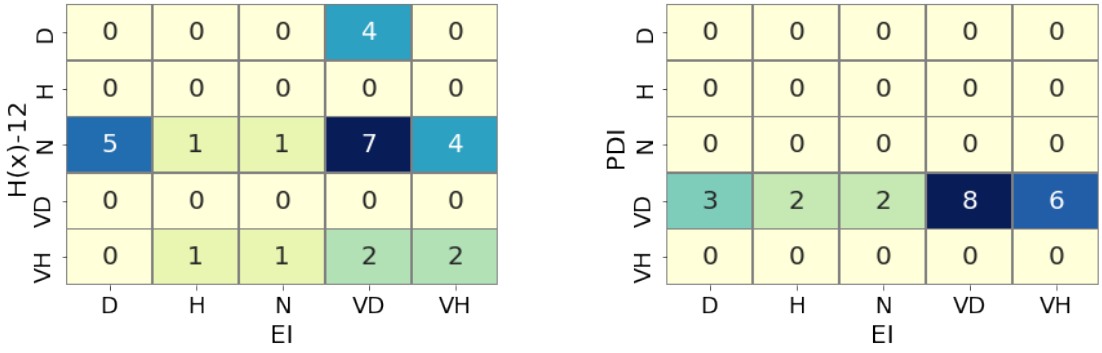

Figure 21: Left : Confusion matrix between EI and H(x)-12 for Mbarek Ben Med H. piezometer. Right : Confusion matrix between EI and PDI for Mbarek Ben Med H. piezometer.

Confusion matrices show near zero accuracy (a = 0.05) for PDI-H(x) classes. Better accuracy is obtained between EI-PDI drought classes for M'barek ben Med H. (a = 0.38). Both piezometers are around 0.10 accuracy for EI-H(x). No predominant class well identified except for EI-PDI for M'barek ben Med H. piezometer with "Very dry" class.

4.4 Raas El Maa groundwater body

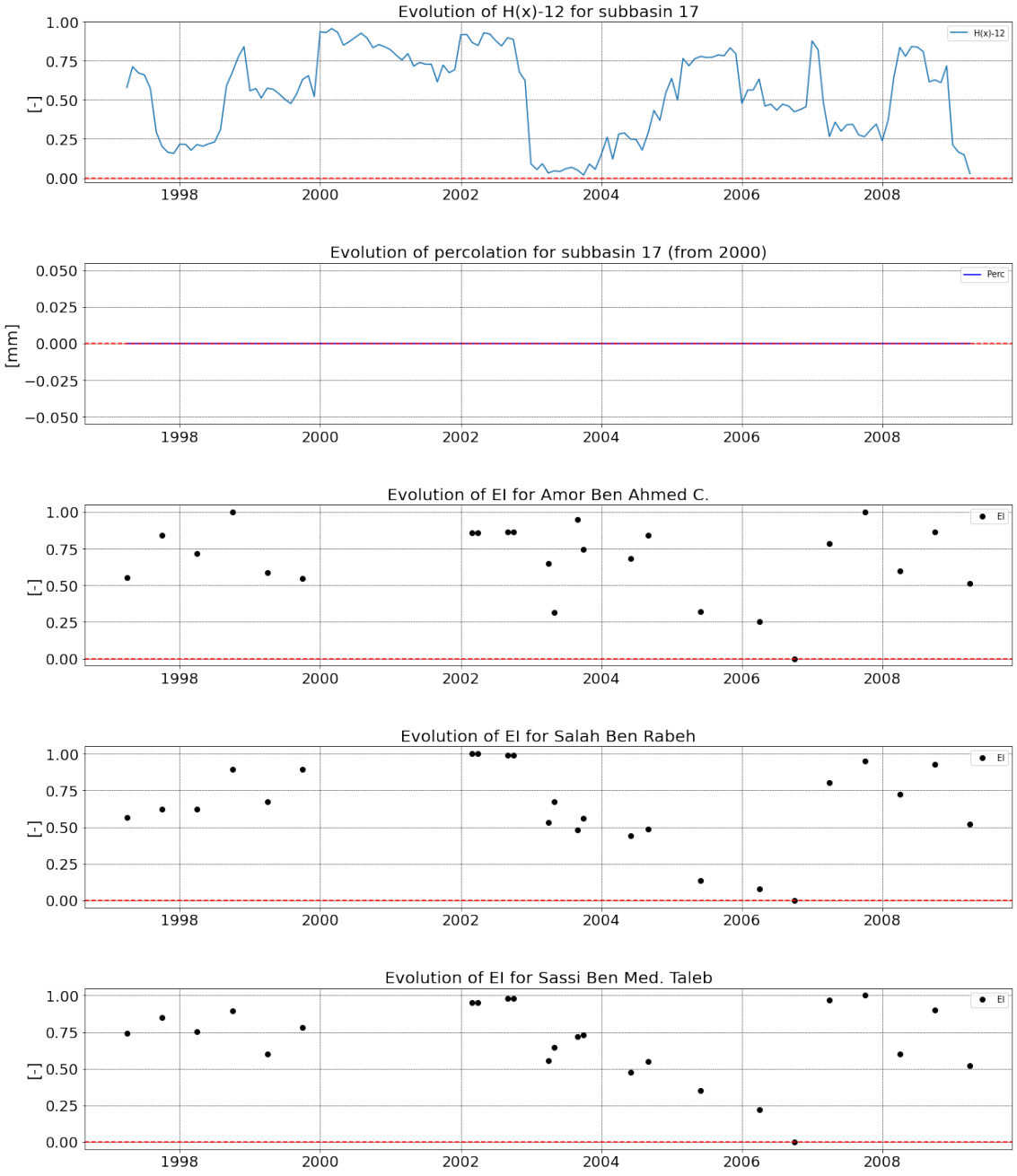

Figure 22: Evolution of H(x)-12, percolation and EI index for piezometers located at Raas El Maa groundwater body.

	H(x)-1	H(x)-3	H(x)-6	H(x)-9	H(x)-12	H(x)-18	H(x)-24
Salah Ben Rabeh	0.325	-0.004	0.252	0.360	0.507	0.505	0.489
Sassi Ben Med. Taleb	0.077	-0.204	0.082	0.166	0.330	0.302	0.326
Amor Ben Ahmed Chelb	-0.072	-0.324	0.065	0.028	0.196	0.032	0.066

Table 26: Spearman's rank correlation coefficient between EI and H(x) for Raas El Maa groundwater .

The Raas el Maa piezometers are located in subbasin 17, characterised by the lowest dominance proportion of wheat crops among all subbasins (30.79%) and complex soils. A middle/high drought pressure is observed during the period 1997-2000 (fig. 22).

There is no recharge observed on this subbasin, suggesting that recharge occurs in other parts of the Siliana catchment. The same evolution of water levels than in other subbasins is noticed. For instance, the recharge of 2003 matches with a reduction of pressure on water resources for all piezometers. In this period high water levels persist until 2006 where the maximum of water table depth is recorded ($EI = 0$). The drought during 2007 matches with a sudden increase of $H(x)$ with a maximum recorded around the end of 2007 ($EI = 1$). After that the drought pressure oscillates between normal and high pressure until the end of records.

Concerning the Spearman's correlation (table 26), all piezometers show the best correlation value for H(x)-12, with a medium correlation for Salah ben Rabeh ($\rho = 0.507$), a weak correlation for Sassi ben Med. Taleb ($\rho = 0.330$) and a very weak correlation for Amor ben Ahmed Chelb ($\rho = 0.196$). The depth of wells can't be relevant because the water levels for the Salah ben Rabeh and Amor Ben Ahmed are more or less at the same depth (respectively 29.06 m and 32.98 m for the lowest level of water table).

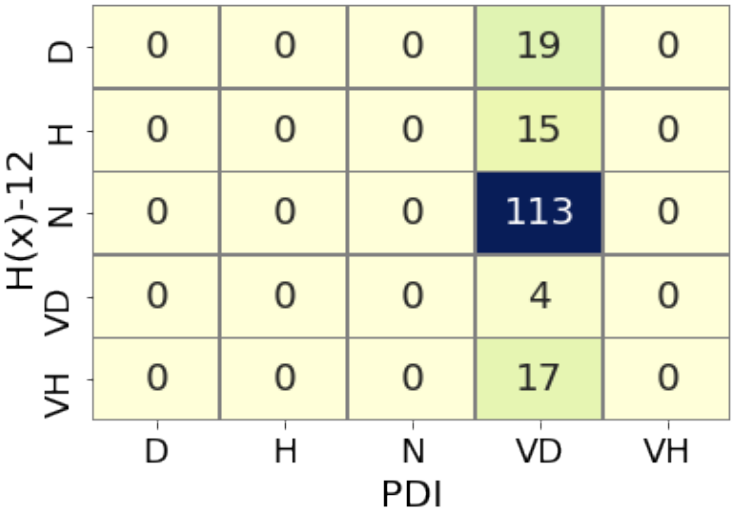

Figure 23: Confusion matrix between H(x)-12 and PDI for subbasin 17.

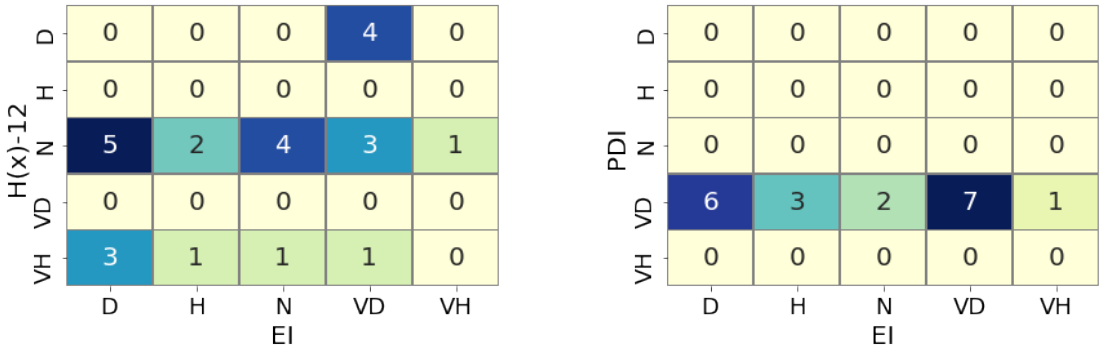

Figure 24: Left : Confusion matrix between EI and H(x)-12 for Amor Ben Ahmed C. piezometer. Right : Confusion matrix between EI and PDI for Amor Ben Ahmed C. piezometer.

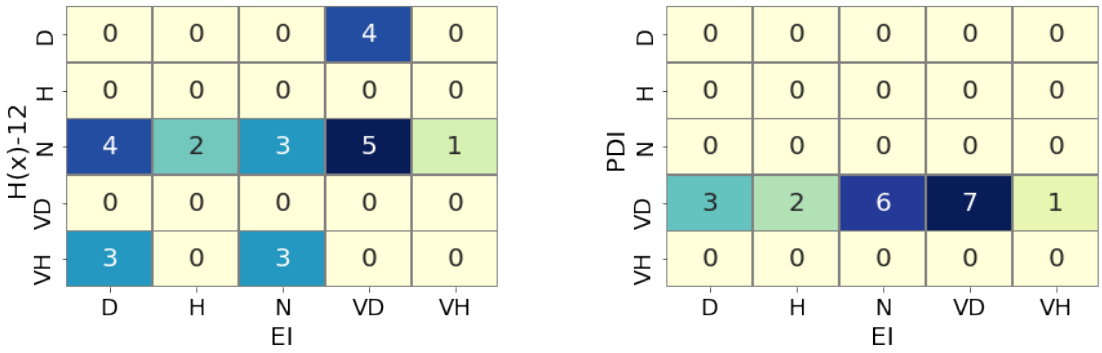

Figure 25: Left : Confusion matrix between EI and H(x)-12 for Sassi Ben Med Taleb piezometer. Right : Confusion matrix between EI and PDI for Sassi Ben Med. Taleb piezometer.

The confusion matrices still show near zero accuracy (a = 0.02) for PDI-H(x) classes and similar accuracy value for both piezometers for EI-PDI classes. The highest value is obtained for Amor ben Ahmed C. between EI-H(x) (a = 0.16)."Normal" class for EI-H(x) and "Very dry" class for EI-PDI are still best coinciding classes.

4.5 Siliana underflow groundwater body

	H(x)-1	H(x)-3	H(x)-6	H(x)-9	H(x)-12	H(x)-18	H(x)-24
PZ 4343 bis/3	-0.118	-0.080	-0.158	0.009	-0.005	0.154	0.241
PZ 4450 bis/3	0.068	-0.039	-0.029	0.049	0.037	0.173	0.161
PZ U2 bis	0.132	0.120	0.063	0.100	0.062	0.258	0.232
PZ P3 BIS	-0.133	-0.110	-0.095	0.056	0.051	0.206	0.279
PZ Saniet Chraiet	-0.015	-0.045	-0.111	0.005	-0.042	0.176	0.312
PZ Romana	-0.062	-0.068	-0.043	0.050	0.083	0.200	0.240
PZ Boukris	-0.167	-0.380	-0.077	0.023	0.041	0.017	0.059

Table 27: Spearman's rank correlation coefficient between EI and H(x) for Siliana Underflow groundwater.

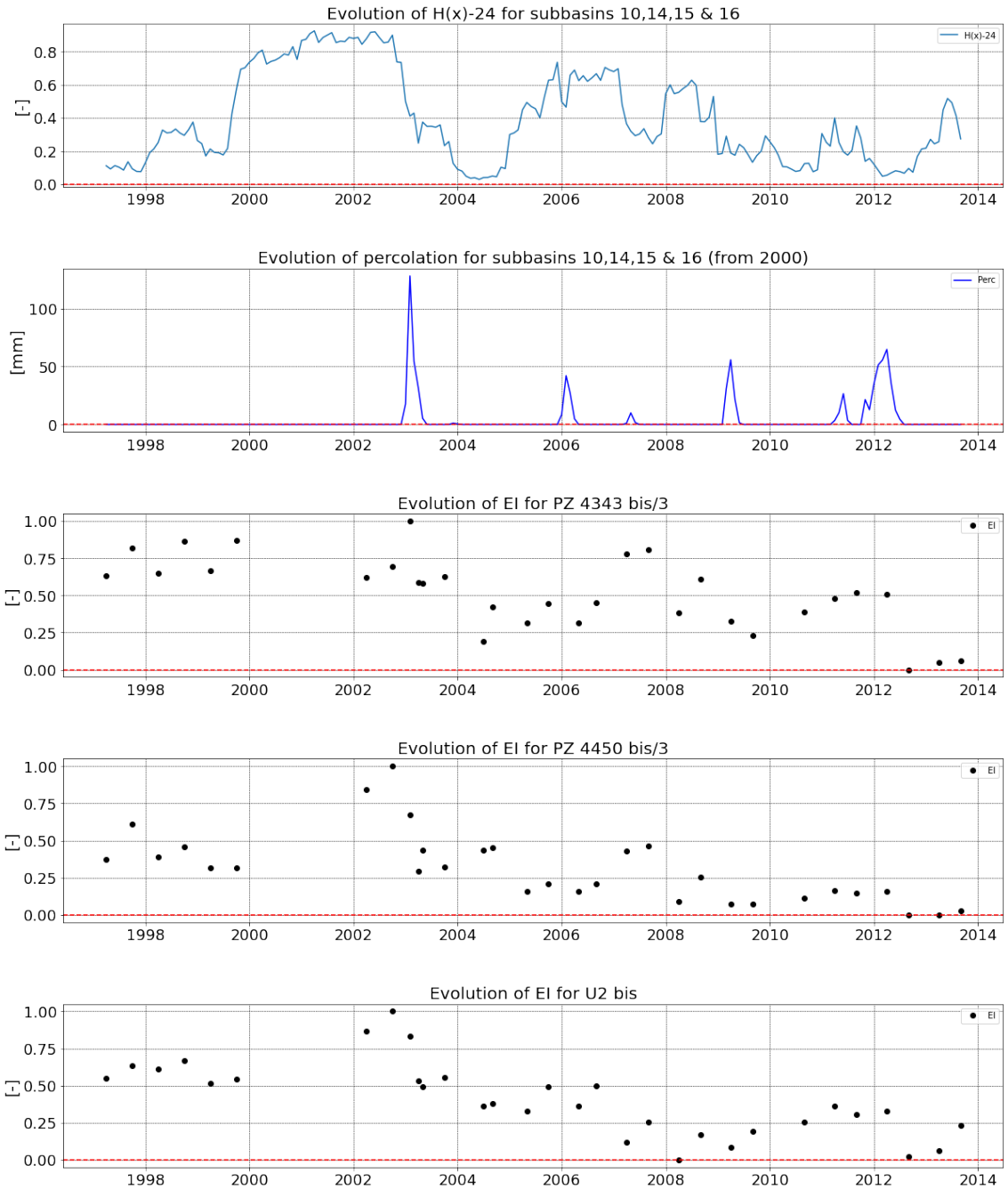

Figure 26: Evolution of H(x)-24, percolation and EI index for piezometers located at Siliana underflow groundwater body (1/2).

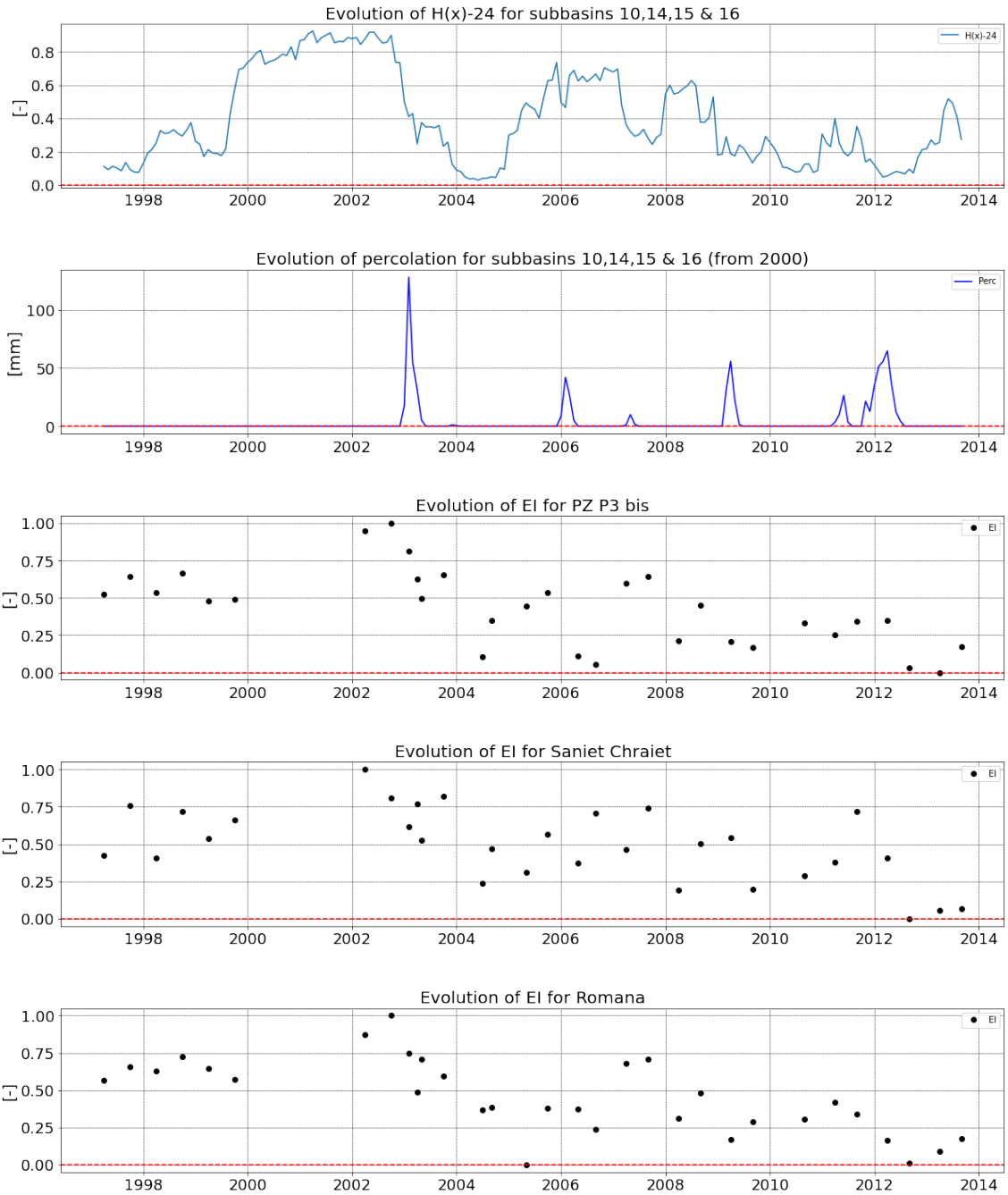

Figure 27: Evolution of H(x)-24, percolation and EI index for piezometers located at Siliana underflow groundwater body (2/2).

The Siliana underflow piezometers are distributed over subbasins 10, 14, 16 and 17. They are characterised by a dominance of wheat crops over all subbasins

and respectively a dominance of vertisols, undeveloped soils, regosols/lithosols and complex soils. Between 1997 and 2000 (fig. 27 and 26), a moderate drought pressure is observed, except for the Boukris piezometer where the EI is below 0.50. At the end of 2002, the drought pressure reaches its maximum value ($EI = 1$) for all piezometers. Then the recharge of 2003 coincides with the decrease of drought pressure. In general the level EI stay below 0.5, except for PZ 4343 and Saniet Chraiet where EI increases above 0.5 after drought of 2010.

Concerning the Spearman's correlation (table 27), the best coefficient appears at H(x)-24, except for PZ 4450 and PZ U2 for which the best results is obtained for $H(x) - 18$) and the PZ Boukris where the best correlation value is attained for $H(x) - 3$. Except for the last one, the coefficient scores are globally lower than those for other groundwater bodies (highest positive value : $\rho = 0.312$). This suggests that depth of the groundwater body affects the sensitivity to drought.

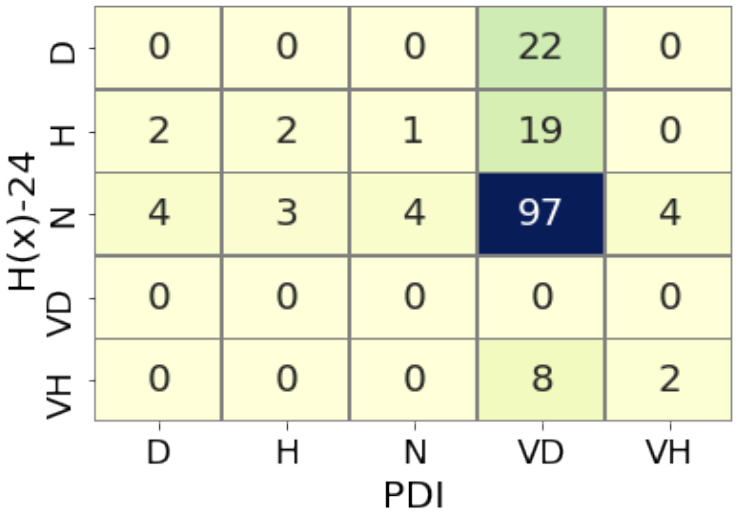

Figure 28: Confusion matrix between H(x)-24 and PDI for subbasins 10, 14, 15 and 16.

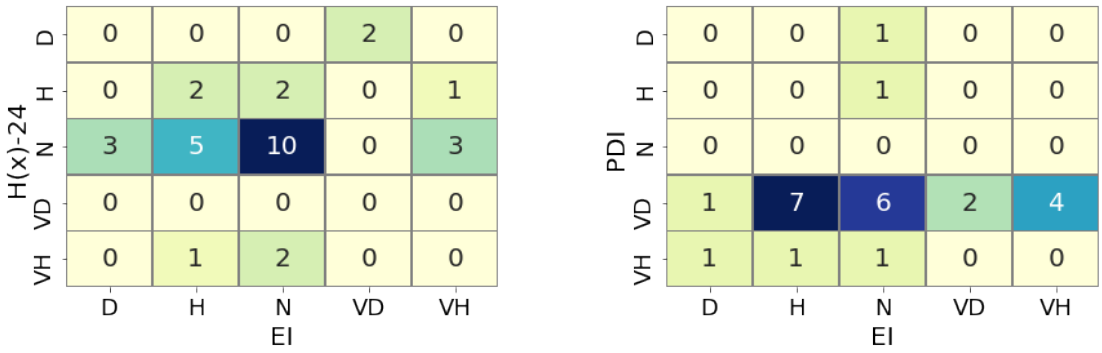

Figure 29: Left : Confusion matrix between EI and H(x)-24 for PZ P3 bis piezometer. Right : Confusion matrix between EI and PDI for PZ P3 bis piezometer.

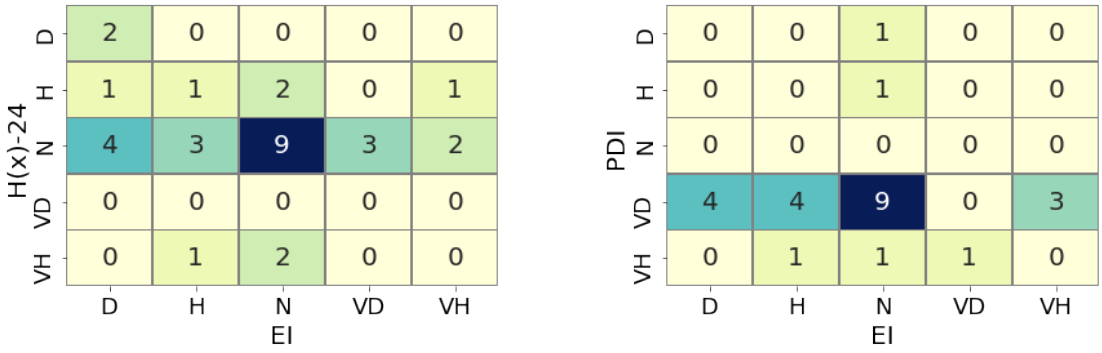

Figure 30: Left : Confusion matrix between EI and H(x)-24 for P2 4343 bis/3 piezometer. Right : Confusion matrix between EI and PDI for PZ 4343 bis/3 piezometer.

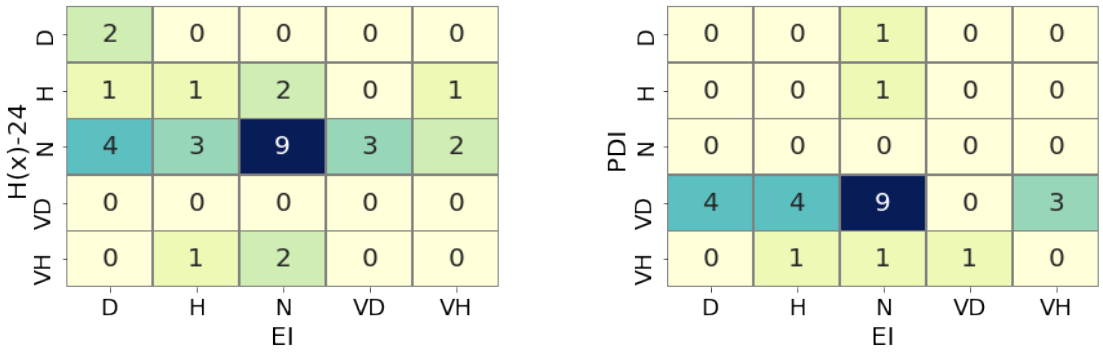

Figure 31: Left : Confusion matrix between EI and H(x)-24 for P2 4450 bis/3 piezometer. Right : Confusion matrix between EI and PDI for PZ 4450 bis/3 piezometer.

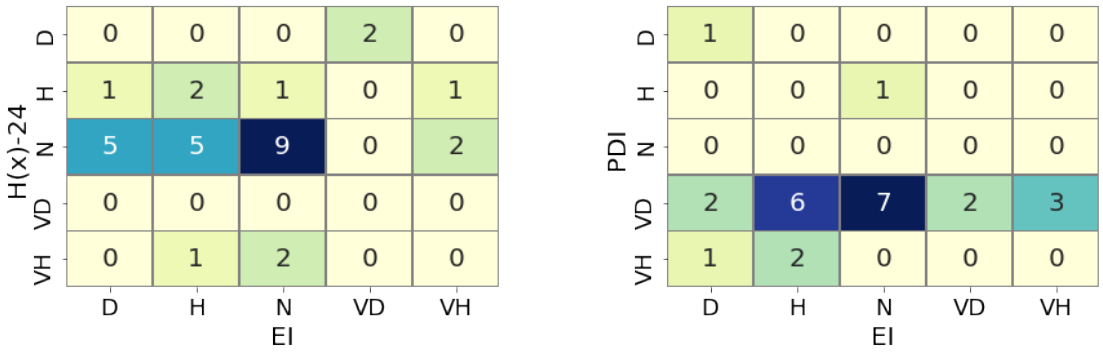

Figure 32: Left : Confusion matrix between EI and H(x)-24 for Romana piezometer. Right : Confusion matrix between EI and PDI for Romana piezometer.

The confusion matrices exhibits again nearly zero accuracy (a = 0.05) for PDI-H(x) drought classes, and very weak accuracy for EI-PDI (a = 0.12), and weak accuracy for EI-H(x) (a = 0.39) for highest scores. All piezometers show best coincidence for "Normal" class between EI and H(x). No specific class is well identified for EI-PDI.

5 Conclusion

In this study, three approaches are implemented and compared to assess drought in the semi-arid Siliana catchment in Tunisia. The first approach (i.e. the approach using the SPI and SPEI-12 indicators) is based on ready available meteorological data. This method is considered as the reference approach. The second and third approaches are based on hydrogeological properties. The second approach uses available piezometric data. In this approach the EI is evaluated. The third approach uses groundwater recharge estimates from a hydrological model. The resulting indicators are compared using rank correlation analysis and confusion matrices.

The comparison between drought assessed with SPI/SPEI-12 and those assessed with EI highlights a constistency in the response of well water to drought. Yet in general a temporal lag is observed between SPI / SPEI and EI. This time lag may be attributed to the delayed reaction time of groundwater when meterological drought is initiated. Yet the evaluation of the EI is subjected to a lot of uncertainty due to the low time resolution of datasets. Most piezometers have only 2 to 4 measurement per year, which could be considered unsufficient for evaluating EI in a robust way. The correlation analysis however show some encouraging results with a reasonable correlation for instance for the "Puits Djelida" piezometer ($\rho = 0.580$). The correlation is further apparently influenced by the depth of the groundwater body. The confusion matrices confirm the analysis made in the correlation analysis. Yet, it may be expected that better results would be obtained if longer datasets with higher temporal resolutions would be available.
The comparisons between drought indices calculated with the hydrological model and indices based on meteorology or piezometry is generally very poor. The simulated recharge insufficiently addresses the persistency of drought as observed with the meteorological based or piezometric based indices.

The study was limited by different methodological aspects. First, the quality of the piezometric data to evaluate the groundwater based drought indicator is poor. The space-time resolution of the available piezometric data is low, and does not allow to have a strong robust estimate of the EI indicator. The uncertainty with the EI indicator could not be assessed in this study. It is therefore recommended to improve the monitoring of groundwater data in the study catchment. Second, the hydrological model to evaluate the recharge based drought indicator does not develop the groundwater component in detail. Indeed, the used SWAT+ model has merely been used and validated to describe the surface flow components of the hydrological cycle, and is not sufficiently adapted to describe the groundwater component. Alternative approaches where SWAT is coupled to a full hydrogeo-

logical model (e.g. MODFLOW) could be proposed to improve the modelling of the groundwater levels and hence the more robust evaluation of the groundwater based drought indicator.

References

[1] Abramopoulos, F., C. Rosenzweig, and B. Choudhury, (1988) : Improved ground hydrology calculations for global climate models (GCMs): Soil water movement and evapotranspiration. J.

[2] Abramowitz, M., and I. A. Stegun (eds.), (1965). Handbook of Mathematical Functions with Formulas, Graphs, and Mathematical Tables. Dover Publications, Inc., New York, New York, 1046 pp.

[3] Aghakouchak, A., Feldman, D., Stewardson, M.J., Saphores, J.D., Grant, S., Sanders, B., (2014). Australia's drought: lessons for California. Science 343 (6178), 1430–1431.

[4] Andreadis, K. M., Clark, E. A., Wood, A. W., Hamlet, A. F., and Lettenmaier, D. P. (2005) : Twentieth-century drought in the conteminous United States, J. Hydrometeorol., 6, 985–1001,

[5] Aouissi, J., Benabdallah, S., Chabaane, Z.L. & Cudennec, C., (2014). Modeling water quality to improve agricultural practices and land management in a tunisian catchment using the soil and water assessment tool. J Environ Qual, 43(1): 18-25.

[6] Arnold, J. G., Srinivasan, R., Muttiah, R. S., & Williams, J. R. (1998). LARGE AREA HYDROLOGIC MODELING AND ASSESSMENT PART I: MODEL DEVELOPMENT. Journal of the American Water Resources Association, 34(1), 73–89.

[7] Bloomfield, J. P.; Marchant, B. P. (2013). Analysis of groundwater drought building on the standardised precipitation index approach. Hydrology and Earth System Sciences, 17(12), 4769–4787.

[8] Chen, Q., Shen, Y., Kusche, J., Chen, W., Chen, T., Zhang, X. (2021). High-resolution GRACE monthly spherical harmonic solutions. Journal of Geophysical Research: Solid Earth, 126, e2019JB018892.

[9] Convention Cadre des Nations Unies sur les Changements Climatiques (CCNUCC) (2018).Troisième Communication Nationale de la Tunisie au titre de la Convention Cadre des Nations Unies sur les Changements Climatiques (CCNUCC).

[10] Croux, C., and Dehon, C. (2010). Influence functions of the Spearman and Kendall correlation measures. Statistical Methods & Applications, 19(4), 497–515.

[11] Darkoh, M.B.K., (2003), The Nature, Causes and Consequences of Desertification in the Drylands of Africa, In: Darkoh, Michael and Apollo Rwomire, Human Impact on Environment and Sustainable Development in Africa , Aldershot: Ashgate Publishers.

[12] Devia, G. K., Ganasri, B. P., & Dwarakish, G. S. (2015). A Review on Hydrological Models. Aquatic Procedia, 4, 1001–1007.

[13] Edwards, D.C. (1997). CHARACTERISTICS OF 20TH CENTURY DROUGHT IN THE UNITED STATES AT MULTIPLE TIME SCALES, Colorado State University.

[14] El Ghoul, I (2017). Modélisation hydrologique du bassin versant de l'Oued Siliana avec le modèle SWAT, Ecole Supérieure des Ingénieurs de Medjez El Bab.

[15] Fareh, A., Burke, S., Werner, M., (2017). Opportunities for complementing data requirements in support of International Policies through the EartH2Observe Water Resources Re-analysis and remotely sensed data products (No. D.2.8). European Commission.

[16] Frappart, F., Ramillien, G. (2018). Monitoring Groundwater Storage Changes Using the Gravity Recovery and Climate Experiment (GRACE) Satellite Mission: A Review. Remote Sensing, 10(6), 829.

[17] Funk, C., Peterson, P., Landsfeld, M. et al. (2015). The climate hazards infrared precipitation with stations—a new environmental record for monitoring extremes. Sci Data 2, 150066.

[18] Funk, C. and Shukla, S., (2020). Drought early warning—definitions, challenges, and opportunities. p. 23-42

[19] Gader K., Gara A., Vanclooster M., Khlifi S. & Slimani M. (2020): Drought assessment in a south Mediterranean transboundary catchment, Hydrological Sciences Journal,

[20] Gordon, A.H. (1992). The random nature of drought: mathematical and physical causes. International Journal of Climatology, 13: 497-507.

[21] Greenwood, J.A., Landwehr, J.M., Matalas, N.C., and Wallis, J.R. (1979). Probability Weighted Moments: Definition and Relation to Parameters of Several Distributions Expressable in Inverse Form, Water Res. Research , vol. 15, no. 5, pp. 1049–1054

[22] Gubareva T.S., Gartsman B. I.(2010). Estimating distribution parameters of extreme hydrometeorological characteristics byL-moments method. , 37(4), 437–445.

[23] Guha-Sapir, D., Hoyois, P., Wallemacq, P., Below, R. (2017). Annual Disaster Statistical Review 2016—The Numbers and Trends. Centre for Research on the Epidemiology of Disasters (CRED).

[24] Guo, M., Yue, W., Wang, T., Zheng, N., Wu, L., (2021). Assessing the use of standardized groundwater index for quantifying groundwater drought over the conterminous US. Journal of Hydrology 598, 126227.

[25] Guttman, N.B. (1994) : On the sensitivity of sample L moments to sample size. Journal of Climate, 7(6):1026–1029

[26] Heim, R. (2002). A Review of Twentieth Century Drought Indices Used in the United States. AMERICAN METEOROLOGICAL SOCIETY.

[27] Hénia, L. (2003). Les grandes sécheresses en Tunisie au cours de la dernière période séculaire In : Eau et environnement : Tunisie et milieux méditerranéens. Lyon : ENS Éditions.

[28] Hisdal, H., Tallasken, L.M. (2000). Drought Event Definition, Technical Report to the ARIDE project No. 6. Department of Geophysics, University of Oslo.

[29] Holzapfel, C. (2008). Deserts. Encyclopedia of Ecology, 879–898.

[30] Hosking, J. R. M. (1990). L-Moments: Analysis and Estimation of Distributions Using Linear Combinations of Order Statistics. Journal of the Royal Statistical Society: Series B (Methodological), 52(1), 105–124.

[31] Jasechko, S., Birks, S. J., Gleeson, T., Wada, Y., Fawcett, P. J., Sharp, Z. D., McDonnell, J. J., & Welker, J. M. (2014). The pronounced seasonality of global groundwater recharge. Water Resources Research, 50(11), 8845-8867.

[32] Jing, W., Zhang, P. & Zhao, X. (2019). A comparison of different GRACE solutions in terrestrial water storage trend estimation over Tibetan Plateau. Sci Rep 9, 1765.

[33] Kumar, R., Musuuza, J. L., Van Loon, A. F., Teuling, A. J., Barthel, R., Ten Broek, J., Mai, J., Samaniego, L., & Attinger, S. (2016) : Multiscale evaluation of the Standardized Precipitation Index as a groundwater drought indicator, Hydrol. Earth Syst. Sci., 20, 1117–1131,

[34] Lana, X., Serra, C., and Burgueño, A. (2001). Patterns of monthly rainfall shortage and excess in terms of the standardized precipitation index for Catalonia (Spain), Int. J. Climatol., 21, 1669–1691.

[35] Landerer, F. W. & Swenson, S. C. (2012). Accuracy of scaled GRACE terrestrial water storage estimates. Water Resources Research 48, 4531

[36] Li, B., Rodell, M. (2014). Evaluation of a model-based groundwater drought indicator in the conterminous U.S. Journal of Hydrology, 526, 78–88.

[37] Limbourg, Lucas. Cartogaphie du potentiel en eau souterraine sur le bassin versant Siliana, Tunisie. Faculté des bioingénieurs, Université catholique de Louvain, 2021. Prom. : Vanclooster, Marnik ; Khlifi, Slaheddine.

[38] Liu, X., Ditmar, P., Siemes, C., Slobbe, D. C., Revtova, E., Klees, R., et al. (2010). DEOS mass transport model (DMT-1) based on GRACE satellite data: Methodology and validation. Geophysical Journal International, 181(2), 769–788.

[39] Long, D., Shen, Y.J., Sun, A., Hong, Y., Longuevergne, L., Yang, Y.T., Li, B., Chen, L., (2014). Drought and flood monitoring for a large karst plateau in Southwest China using extended GRACE data. Remote Sens. Environ. 155, 145–160.

[40] Maliva, R., Missimer, T. (2012). Arid Lands Water Evaluation and Management, Environmental Science and Engineering,

[41] Margat, J. and van der Gun, J. (2013). Groundwater around the World: A Geographic Synopsis. CRC Press/Balkema. Leiden, pp. 124-125

[42] Mavromatis, T.. (2007). Drought index evaluation for assessing future wheat production in Greece. International Journal of Climatology. 27. 911 - 924. 10.1002/joc.1444.

[43] McKee, T. B., Doesken, N. J., and Leist, J. (1993) : The relationship of drought frequency and duration time scales, 8th Conference on Applied Climatology, 17–22 January 1993, Anaheim, California, 179–184.

[44] Middleton N., Thomas D. (1997). World Atlas of Desertification, 2nd edn, Arnold E (ed). UNEP, Hodder Headline plc.: London

[45] Mjejra M., (2015). Étude de l'évapotranspiration dans le bassin versant de Mejerda (en Tunisie) : apport de la télédétection satellitaire et des

Systèmes d'Information Géographique. Géographie. Université Rennes 2. Français. ffNNT : 2015REN20050ff. fftel-01281636

[46] Neitsch, S.I., Arnold, J.G., Kiniry, J.R. & Williams, J.R., (2005). Soil and water assessment tool theoretical documentation, version 2005. Temple, TX: US Department of Agriculture, Agricultural Research Service, Grassland, Soil and Water Research Laboratory

[47] Nunez, J. Verbist, Koen Wallis, Jim Schaefer, M. Morales-Salinas, Luis Cornelis, Wim. (2011). Regional frequency analysis for mapping drought events in north-central Chile. Journal of Hydrology. 405. 352-366. 10.1016/j.jhydrol.2011.05.035.

[48] Observatoire du Sahara et du Sahel (OSS), Vers un système d'alerte précoce à la sécheresse au Maghreb (2008), Collection Synthèse n° 4. Tunis, pp. 84

[49] Ouessar, M., Bruggeman, A., Abdelli, F., Mohtar, R.H., Gabriels, D. & Cornelis, W.M., (2009). Modelling water-harvesting systems in the arid south of Tunisia using SWAT. Hydrology and Earth System Sciences 13(10): 2003-2021.

[50] Ozenda, P. (1975) : Sur les étages de végétation dans les montagnes du Bassin Méditerranéen. Documents de Cartographie Ecologique, 16, pp. 1-32.

[51] Panofsky, H. A., and G. W. Brier, (1958). Some Applications of Statistics to Meteorology. Earth and Mineral Sciences Continuing Education, College of Earth and Mineral Sciences, The Pennsylvania State University, University Park, Pennsylvania, 224 PP.

[52] RAPPORT NATIONAL DU SECTEUR DE L'EAU (2019),Ministère de l'Agriculture, des Ressources Hydrauliques et de la Pêche, République Tunisienne.

[53] Rodell, M., Famiglietti, J.S., (1999). Detectability of variations in continental water storage from satellite observations of the time dependent gravity field. Water Resour. Res. 35 (9).

[54] Rowlands, D.D., Luthcke, S.B., Klosko, S.M., Lemoine, F.G.R., Chinn, D.S., McCarthy, J.J., Cox, C.M., Anderson, O.B., (2005). Resolving mass flux at high spatial and temporal resolution using GRACE intersatellite measurements. Geophys. Res. Lett. 32, L04310.

[55] Sakumura, C., Bettadpur, S., Bruinsma, S. (2014). Ensemble prediction and intercomparison analysis of GRACE time-variable gravity field models. Geophysical Research Letters, 41(5), 1389–1397.

[56] Samaniego, L., Kumar, R., and Zink, M. (2013) : Implications of parameter uncertainty on soil moisture drought analysis in Germany, J. Hydrometeorol., 14, 47–68.

[57] Scanlon, B. R., Zhang, Z., Save, H., Sun, A. Y., Müller Schmied, H., van Beek, L. P. H., ... Bierkens, M. F. P. (2018). Global models underestimate large decadal declining and rising water storage trends relative to GRACE satellite data. Proceedings of the National Academy of Sciences, 115(6), E1080–E1089.

[58] Sellami, H., La Jeunesse, I., Benabdallah, S., Baghdadi, N. & Vanclooster, M., (2014). Uncertainty analysis in model parameters regionalization: a case study involving the SWAT model in Mediterranean catchments (Southern France). Hydrology and Earth System Sciences, 18(6): 2393-2413.

[59] Sellami, H., Benabdallah, S., La Jeunesse, I. & Vanclooster, M., (2016). Climate models and hydrological parameter uncertainties in climate change impacts on monthly runoff and daily flow duration curve of a Mediterranean catchment. Hydrological Sciences Journal, 61(8): 1415-1429.

[60] Sellami, H., Khlifi, S. & Vanclooster, M. (2021). Drought Regional Frequency Mapping in Tunisia.3rd Atlas Georesources International Congress (AGIC 2021) (www, du 22/03/21 au 24/03/21). In: Water Quality, Global Changes and Grounwater Responses.

[61] Sheffield, J., Goteti, G., Wen, F., and Wood, E. F (2004).: A simulated soil moisture based drought analysis for the United States, J. Geophys. Res., 109, D24108.

[62] Sheffield, J., Goteti, G., Wood, E. (2006). Development of a 50-Year High-Resolution Global Dataset of Meteorological Forcings for Land Surface Modeling. Journal of Climate, 19, 3088-3111.

[63] Sheffield, J., Wood, E.F., (2012). Drought: Past Problems and Future Scenarios. Routledge. Shukla

[64] Sinha, D., Syed, T.H., Reager, J.T., (2019). Utilizing combined deviations of precipitation and GRACE-based terrestrial water storage as a metric for

drought characterization: a case study over major Indian river basins. J. Hydrol. 572, 294–307.

[65] Soong T.T. (2004), "Fundamentals of Probability and Statistics for Engineers", John Wiley Sons Ltd, State University of New York at Buffalo, Buffalo, New York, USA.

[66] Spearman C., (1904). General intelligence objectively determined and measured. Am J Psychol 15:201–293

[67] Spinoni J, Naumann G, Carrão H, Barbosa Ferreira P, Vogt J. (2014) Towards identifying areas at climatological risk of desertification using the Köppen–Geiger classification and FAO aridity index . INTERNATIONAL JOURNAL OF CLIMATOLOGY 35 (9); p. 2210-2222. JRC83589

[68] Swenson, S. C. (ed. PO.DAAC) (CA, USA, 2012).

[69] Thom, H. C. S., (1966). Some Methods of Climatological Analysis. WMO Technical Note Number 81, Secretariat of the World Meteorological Organization, Geneva, Switzerland, 53 pp

[70] Thomas, B. F., Famiglietti, J. S., Landerer, F. W., Wiese, D. N., Molotch, N. P., Argus, D. F. (2017). GRACE Groundwater Drought Index: Evaluation of California Central Valley groundwater drought. Remote Sensing of Environment, 198, 384–392.

[71] Thomas, A. C., Reager, J. T., Famiglietti, J. S., Rodell, M. (2014). A GRACE-based water storage deficit approach for hydrological drought characterization. Geophysical Research Letters, 41(5), 1537–1545.

[72] Thornthwaite, C. W., (1948) : An approach toward a rational classification of climate. Geogr. Rev., 38, 55–94.

[73] Thornthwaite, C.W., Mather, J.R., (1955). The Water Balance. Publ. in Climatology, 8(1), C.W Thornthwaite and Associates, Centerton, New Jersey.

[74] Thornthwaite, C.W., Mather, J.R., (1957). Instructions and Tables for-Computing Potential Evapotranspiration and the Water Balance. Publ. in Climatology, 10(3), C.W. Thornthwaite and Associates, Centerton, New Jersey.

[75] United Nations Environment Programme (UNEP) (1997). World atlas of desertification 2ED. UNEP, London.

[76] USDA-NRCS, (2004). Chapter 10: Estimation of direct runoff from storm rainfall. In: NRCS National Engineering Handbook, Part 630: Hydrology. U.S. Department of Agriculture, Natural Resources Conservation Service, Washington, DC.

[77] Van Camp, M., Radfar, M., Walraevens, K. (2010). Assessment of groundwater storage depletion by overexploitation using simple indicators in an irrigated closed aquifer basin in Iran. Agricultural Water Management, 97(11), 1876–1886.

[78] Varouchakis, E.A., Corzo, G.A., Karatzas, G.P. et al. (2018). Spatio-temporal analysis of annual rainfall in Crete, Greece. Acta Geophys. 66, 319–328. https://doi.org/10.1007/s11600-018-0128-z

[79] Verstraete, M. M. (1986). DEFINING DESERTIFICATION: .4, REVIEW. Climatic Change, 9, 5–18.

[80] Vicente-Serrano, S., Begueria, S., Lopez-Moreno, J. (2010). A Multiscalar Drought Index Sensitive to Global Warming: The Standardized Precipitation Evapotranspiration Index. Journal of Climate, 23, 1696–1718.

[81] Vidal, J.-P., Martin, E., Franchistéguy, L., Habets, F., Soubeyroux, J.-M., Blanchard, M., and Baillon, M. (2010) : Multilevel and multiscale drought reanalysis over France with the Safran-IsbaModcou hydrometeorological suite, Hydrol. Earth Syst. Sci., 14, 459–478.

[82] Vrbo, J., Lippanen, A. (Eds.), (2007). Groundwater Resources Sustainability Indicators. UNESCO, Paris.

[83] Wahr, J., Swenson, S., Velicogna, I., (2006). Accuracy of GRACE mass estimates. Geophys. Res. Lett. 33 (6).

[84] Watkins, M. M., Wiese, D. N., Yuan, D. N., Boening, C. & Landerer, F. W. (2015) : Improved methods for observing Earth's time variable mass distribution with GRACE using spherical cap mascons. Journal of Geophysical Research Solid Earth 120, 2648–2671.

[85] Wilhite, D., Glantz, M., (1985). Understanding the Drought Phenomenon: The Role of Definitions, vol. 10. Drought Mitigation Center Faculty Publications, pp. 111-120.

[86] Wilhite, D., Svoboda, M., Hayes, M. (2007). Understanding the Complex Impacts of Drought: A Key to Enhancing Drought Mitigation and Preparedness. Water Resources Management, 21, 763–774.

[87] Willmott, C.J., (1977). Watbug: A FORTRAN IV Algorithm for Calculating the Climatic Water Budget. Publications in Climatology 30, C.W. Thornthwaite Assoc., Laboratory of Climatology, Elmer, NJ, p. 55.

[88] World Meteorological Organization (WMO), (2012) Standardized Precipitation Index User Guide No. 1090, p. 24.

[89] Zhang, Y., Li, W., Chen, Q. et al. (2017). Multi-models for SPI drought forecasting in the north of Haihe River Basin, China. Stoch Environ Res Risk Assess 31, 2471–2481.

Appendix

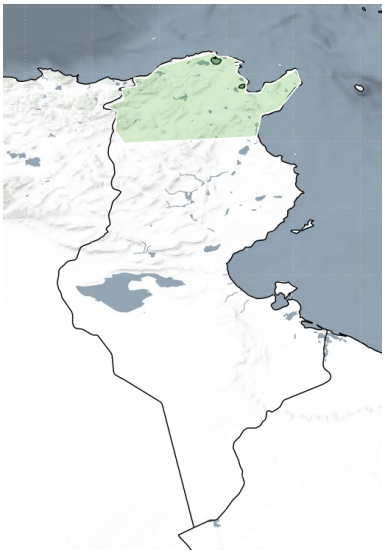

Figure 33: Region selected for North Tunisia on WCI

Figure 34: Region selected for Central Tunisia on WCI

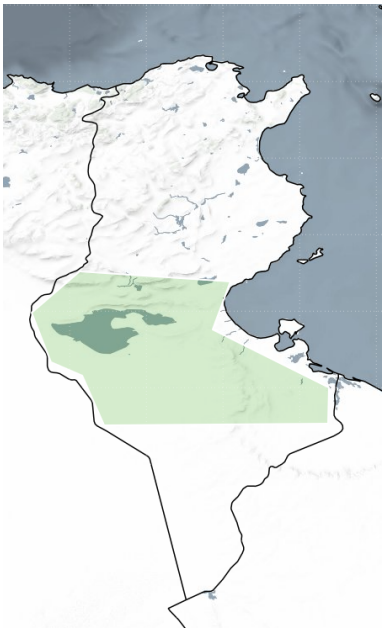

Figure 35: Region selected for South Tunisia on WCI

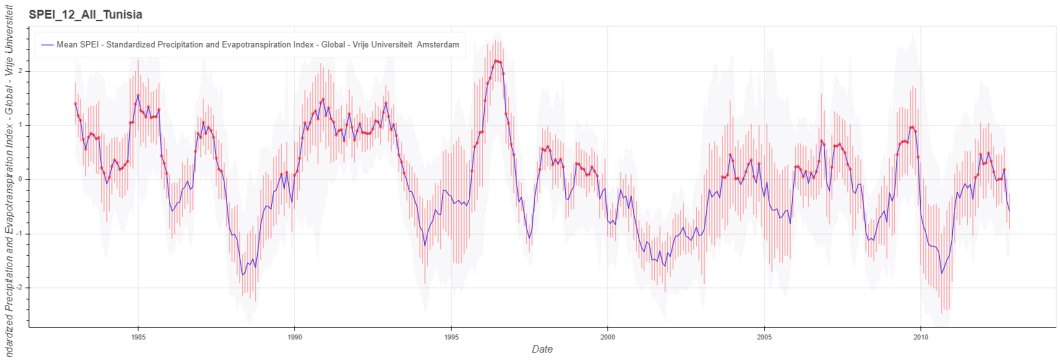

Figure 36: SPEI for Tunisia from 1983-2012 generated on WCI

Year	Hénia	EMDAT
1900-1901	South	
1901-1902	South	
1907-1908	Tunisia	
1909-1910	Center	
1911-1912	North	
1913-1914	Tunisia	
1915-1916	South	
1917-1918	North	
1918-1919	Center	
1919-1920	South	
1921-1922	Tunisia	
1923-1924	South	
1924-1925	North	
1925-1926	South	
1926-1927	Tunisia	
1929-1930	North & South	
1930-1931	Center & South	
1933-1934	South	
1935-1936	Center & South	
1936-1937	South	
1937-1938	Center	
1939-1940	South	
1940-1941	Center	
1941-1942	South	
1942-1943	North	
1943-1944	North & South	
1944-1945	Tunisia	
1945-1946	Center	
1946-1947	North	
1947-1948	North & South	
1949-1950	South	
1950-1951	Tunisia	
1953-1954	South	
1954-1955	North & Center	
1959-1960	North	
1960-1961	Tunisia	
1961-1962	Center & South	
1965-1966	North	
1966-1967	North	
1968-1969	Tunisia	
1970-1971	South III	
1976-1977	South	Center & South (1977)

Table 28: Drought episodes from 1900-1901 to 1979-1980

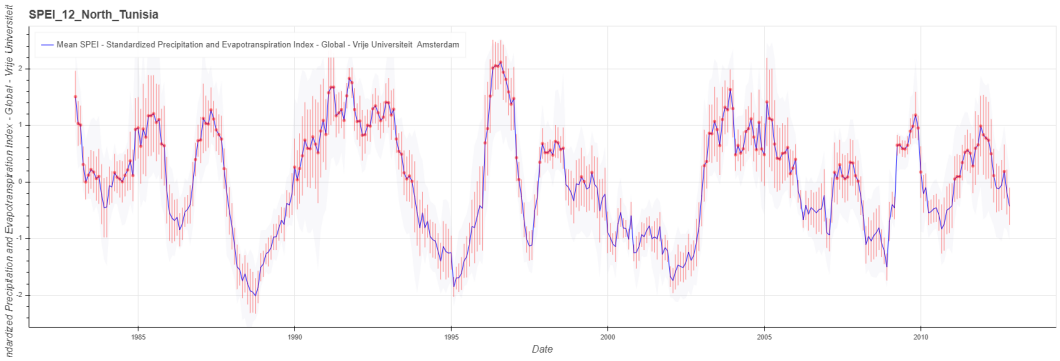

Figure 37: SPEI for North Tunisia from 1983-2012 generated on WCI

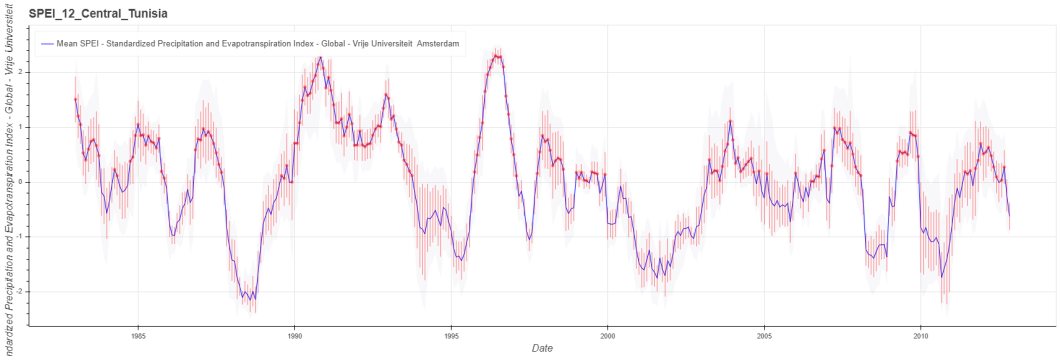

Figure 38: SPEI for Central Tunisia from 1983-2012 generated on WCI

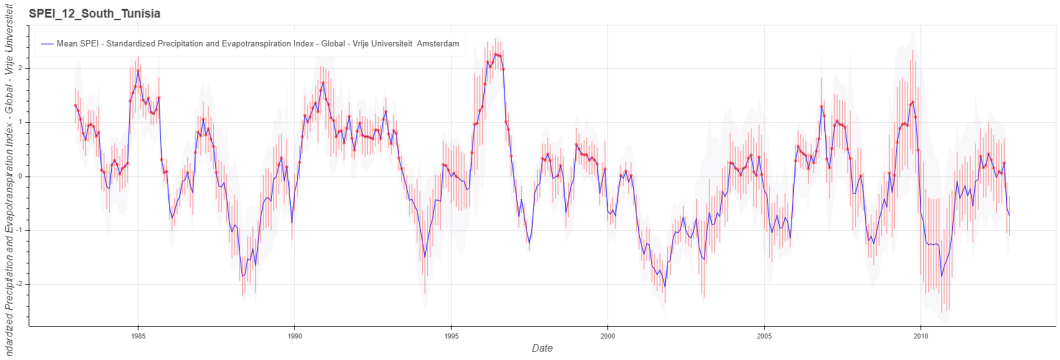

Figure 39: SPEI for South Tunisia from 1983-2012 generated on WCI

Figure 40: SPI for Tunisia from 1983-2012 generated on WCI

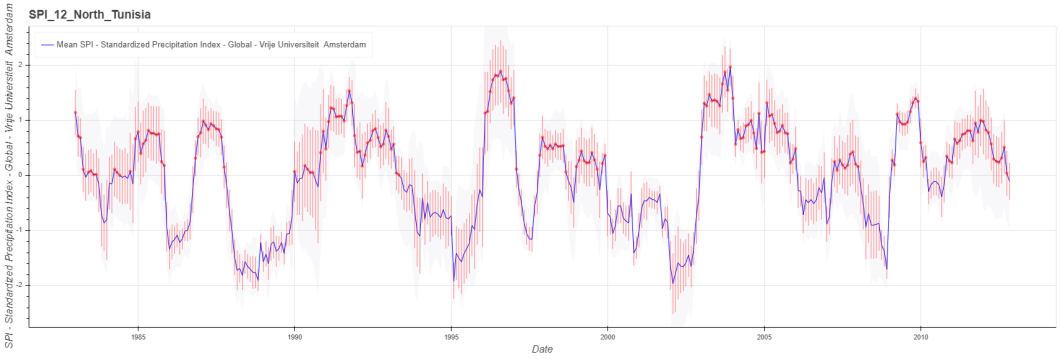

Figure 41: SPI for North Tunisia from 1983-2012 generated on WCI

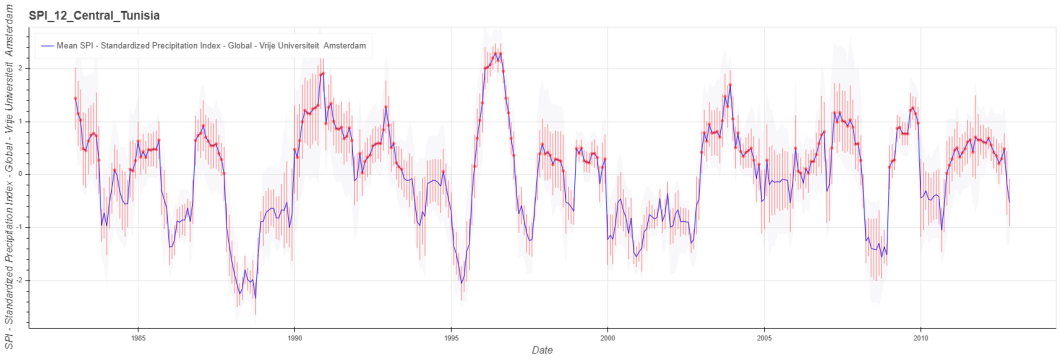

Figure 42: SPI for Central Tunisia from 1983-2012 generated on WCI

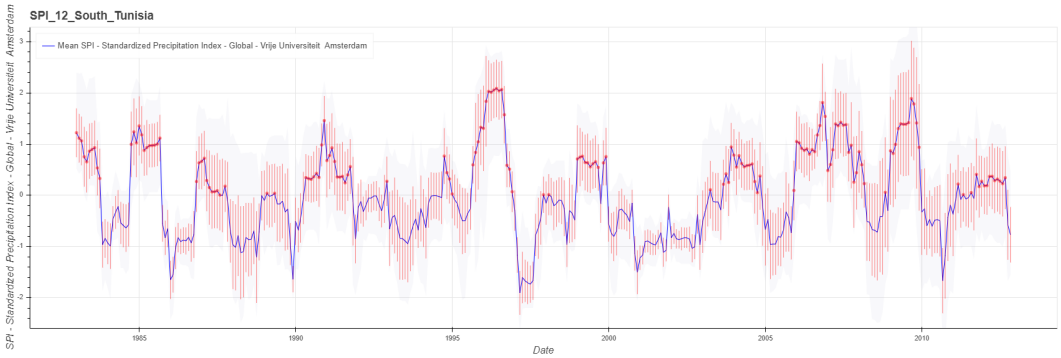

Figure 43: SPI for South Tunisia from 1983-2012 generated on WCI

Code_Preci_CHIRPS_PENTAD *

```
Imports (1 entry)
  var polygon: Table users/WailSemlali/Subbasin_9
var shp = ee.FeatureCollection(polygon);

Map.addLayer(shp, {}, 'My polygon');

var image = ee.ImageCollection("UCSB-CHG/CHIRPS/PENTAD");
var dataset= image.filterDate('2014-01-01','2020-12-31');

print(dataset);

var preci=dataset.map(function(dataset){
                        return dataset.clip(polygon);
                      });
var precipitation = preci.select('precipitation');

print(precipitation,'precipitation');

Map.addLayer(precipitation);
```

Figure 44: GEE code for CHIRPS precipitation data.

SAMPLE SIZE (N)	LEVEL OF SIGNIFICANCE FOR D = MAXIMUM [$F_0(X)$ - $S_n(X)$]				
	.20	.15	.10	.05	.01
1	.900	.925	.950	.975	.995
2	.684	.726	.776	.842	.929
3	.565	.597	.642	.708	.828
4	.494	.525	.564	.624	.733
5	.446	.474	.510	.565	.669
6	.410	.436	.470	.521	.618
7	.381	.405	.438	.486	.577
8	.358	.381	.411	.457	.543
9	.339	.360	.388	.432	.514
10	.322	.342	.368	.410	.490
11	.307	.326	.352	.391	.468
12	.295	.313	.338	.375	.450
13	.284	.302	.325	.361	.433
14	.274	.292	.314	.349	.418
15	.266	.283	.304	.338	.404
16	.258	.274	.295	.328	.392
17	.250	.266	.286	.318	.381
18	.244	.259	.278	.309	.371
19	.237	.252	.272	.301	.363
20	.231	.246	.264	.294	.356
25	.210	.220	.240	.270	.320
30	.190	.200	.220	.240	.290
35	.180	.190	.210	.230	.270
OVER 35	$\frac{1.07}{\sqrt{N}}$	$\frac{1.14}{\sqrt{N}}$	$\frac{1.22}{\sqrt{N}}$	$\frac{1.36}{\sqrt{N}}$	$\frac{1.63}{\sqrt{N}}$

Figure 45: Critical value for Kolmogorov-Smirnov test
Source:http://people.cs.pitt.edu/ lipschultz/cs1538/prob-table$_K S.pdf$

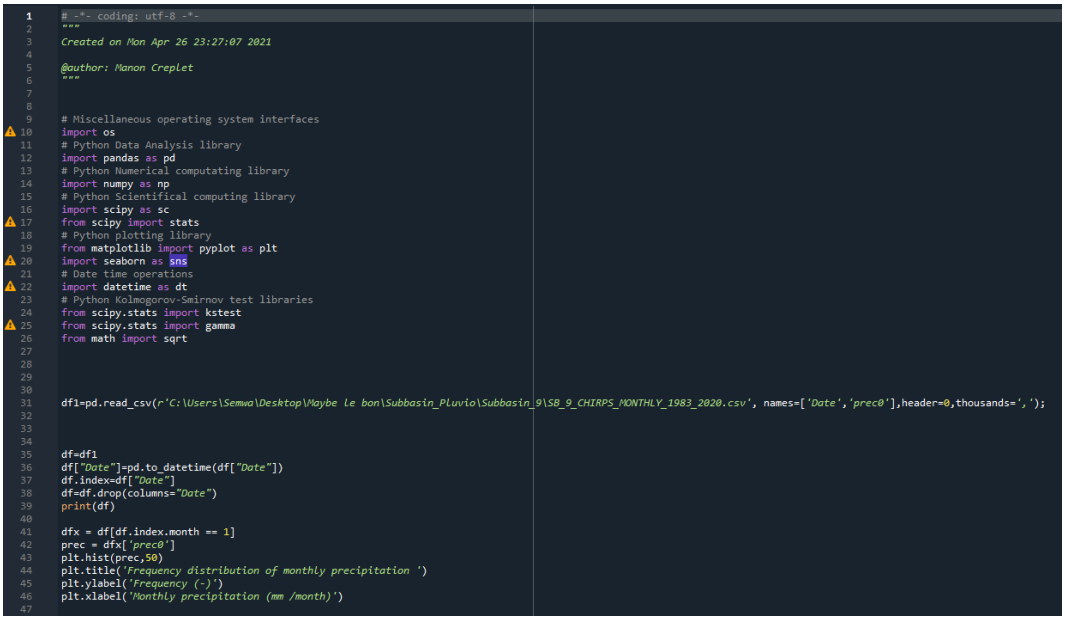

```python
# -*- coding: utf-8 -*-
"""
Created on Mon Apr 26 23:27:07 2021

@author: Manon Creplet
"""


# Miscellaneous operating system interfaces
import os
# Python Data Analysis library
import pandas as pd
# Python Numerical computating library
import numpy as np
# Python Scientifical computing library
import scipy as sc
from scipy import stats
# Python plotting library
from matplotlib import pyplot as plt
import seaborn as sns
# Date time operations
import datetime as dt
# Python Kolmogorov-Smirnov test libraries
from scipy.stats import kstest
from scipy.stats import gamma
from math import sqrt




df1=pd.read_csv(r'C:\Users\Semwa\Desktop\Maybe le bon\Subbasin_Pluvio\Subbasin_9\SB_9_CHIRPS_MONTHLY_1983_2020.csv', names=['Date','prec0'],header=0,thousands=',');



df=df1
df["Date"]=pd.to_datetime(df["Date"])
df.index=df["Date"]
df=df.drop(columns="Date")
print(df)

dfx = df[df.index.month == 1]
prec = dfx['prec0']
plt.hist(prec,50)
plt.title('Frequency distribution of monthly precipitation ')
plt.ylabel('Frequency (-)')
plt.xlabel('Monthly precipitation (mm /month)')

```

Figure 46: Python code on Spyder for Kolmogorov-Smirnov test with gamma distribution(1/2) (Creplet, 2021)

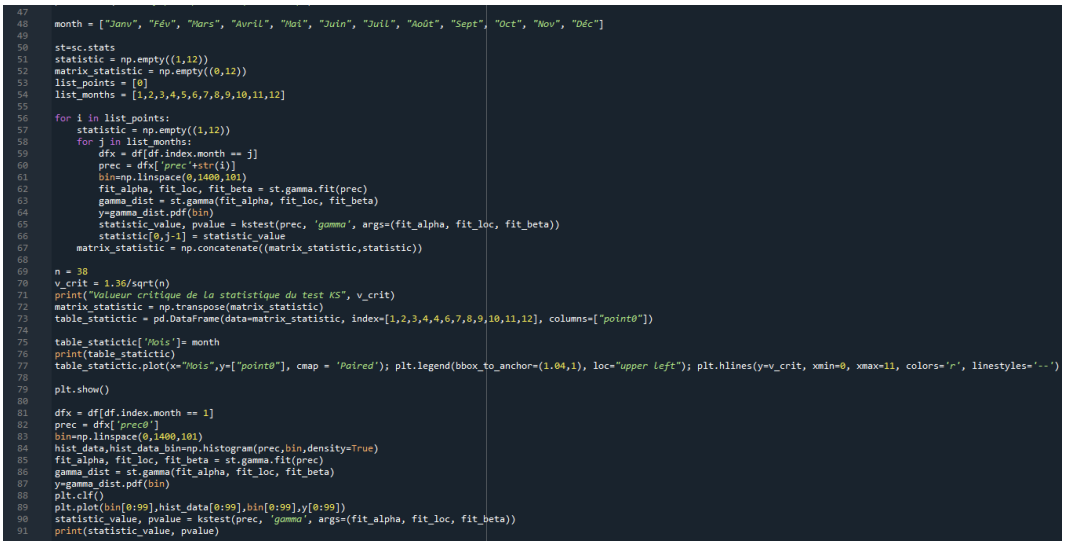

```python

month = ["Janv", "Fév", "Mars", "Avril", "Mai", "Juin", "Juil", "Août", "Sept", "Oct", "Nov", "Déc"]

st=sc.stats
statistic = np.empty((1,12))
matrix_statistic = np.empty((0,12))
list_points = [0]
list_months = [1,2,3,4,5,6,7,8,9,10,11,12]

for i in list_points:
    statistic = np.empty((1,12))
    for j in list_months:
        dfx = df[df.index.month == j]
        prec = dfx['prec'+str(i)]
        bin=np.linspace(0,1400,101)
        fit_alpha, fit_loc, fit_beta = st.gamma.fit(prec)
        gamma_dist = st.gamma(fit_alpha, fit_loc, fit_beta)
        y=gamma_dist.pdf(bin)
        statistic_value, pvalue = kstest(prec, 'gamma', args=(fit_alpha, fit_loc, fit_beta))
        statistic[0,j-1] = statistic_value
    matrix_statistic = np.concatenate((matrix_statistic,statistic))

n = 38
v_crit = 1.36/sqrt(n)
print("Valueur critique de la statistique du test KS", v_crit)
matrix_statistic = np.transpose(matrix_statistic)
table_statictic = pd.DataFrame(data=matrix_statistic, index=[1,2,3,4,4,6,7,8,9,10,11,12], columns=["point0"])

table_statictic['Mois']= month
print(table_statictic)
table_statictic.plot(x="Mois",y=["point0"], cmap = 'Paired'); plt.legend(bbox_to_anchor=(1.04,1), loc="upper left"); plt.hlines(y=v_crit, xmin=0, xmax=11, colors='r', linestyles='--')

plt.show()

dfx = df[df.index.month == 1]
prec = dfx['prec0']
bin=np.linspace(0,1400,101)
hist_data,hist_data_bin=np.histogram(prec,bin,density=True)
fit_alpha, fit_loc, fit_beta = st.gamma.fit(prec)
gamma_dist = st.gamma(fit_alpha, fit_loc, fit_beta)
y=gamma_dist.pdf(bin)
plt.clf()
plt.plot(bin[0:99],hist_data[0:99],bin[0:99],y[0:99])
statistic_value, pvalue = kstest(prec, 'gamma', args=(fit_alpha, fit_loc, fit_beta))
print(statistic_value, pvalue)
```

Figure 47: Python code on Spyder for Kolmogorov-Smirnov test with gamma distribution(2/2) (Creplet, 2021)

In [2]:
```
import numpy as np
import scipy as sc
import pandas as pd
import matplotlib.pyplot as plt
plt.rcParams["figure.figsize"]=20,12
```

In [5]:
```
df1 = pd.read_csv('SB_2_4_Hx_9.csv', names=['Date','Hx'], header=0)
df2 = pd.read_csv('Youssef_Lab_EI.csv', names=['Date','EI'], header=0)
df1['Hx'] = pd.to_numeric(df1['Hx'], downcast="float")
df2['EI'] = pd.to_numeric(df2['EI'], downcast="float")
df1['Date'] = pd.to_datetime(df1['Date'])
df2['Date'] = pd.to_datetime(df2['Date'])
```

In [7]:
```
#df1[df1['Date'] > '1995-01-01'].plot()
selected_dates = df1['Date'] > '1995-01-01'
plt.plot(df1[selected_dates]['Date'], df1[selected_dates]['Hx'])
#plt.plot(df1['Date'], df1['Hx'])
plt.plot(df2['Date'], df2['EI'], 'o', color='black')


plt.axhline(y=0, color='r', linestyle='--')
plt.title('H(x)/EI evolution for Youssef Lab PZ')
plt.grid(color = 'black', linestyle = '--', linewidth=0.5)

plt.legend(["H(x)", "EI"])
```

Figure 48: Python code on Jupyter Notebook for correlation plot and test between H(x) and EI (1/4)

In [16]:
```
import numpy as np
import pandas as pd
from pandas import Series, DataFrame
import matplotlib.pyplot as plt

from pylab import rcParams
import seaborn as sb

import scipy
from scipy.stats import spearmanr
```

In [17]:
```
df1 = pd.read_csv('SB_16_Hx_6.csv', names=['Date','Hx'], header=0)
df2 = pd.read_csv('Abdelmlek_EI.csv', names=['Date','EI'], header=0)

df1.merge(df2, how='inner', on=['Date'])
# utiliser inner join (= nom d'un opérateur
#algébrique sur l'algèbre sigma) pour fusionner
#2 colonnes de 2 sets differents sur base de la meme date
#df3 = pd.read_csv('Merged_data_FI_Hx.csv', names= ['Nan','Date','Hx','FI'], header=0)
df3 = df1.merge(df2, how='inner', on=['Date'])

f3.drop(columns="Nan") #jarter colonne
```

In [18]:
```
df3
```

Out[18]:

	Date	Hx	EI
0	Apr 1, 1998	0.520	0.000000
1	Oct 1, 1998	0.665	0.000000
2	Apr 1, 1999	0.356	0.727891
3	Oct 1, 1999	0.861	0.965986
4	Apr 1, 2003	0.009	0.732077
5	Oct 1, 2003	0.408	0.746206
6	Apr 1, 2004	0.288	0.413396
7	Oct 1, 2004	0.789	0.499738
8	Apr 1, 2005	0.674	0.421769
9	Oct 1, 2005	0.889	0.510727
10	Apr 1, 2006	0.385	0.427002
11	Oct 1, 2006	0.571	0.512297
12	Apr 1, 2007	0.191	0.965986

Figure 49: Python code on Jupyter Notebook for correlation plot between H(x) and EI (2/4)

```
In [11]: df3.plot(x='Hx', y='EI', style ='o')
```

```
Out[11]: <matplotlib.axes._subplots.AxesSubplot at 0x172d00ac0a0>
```

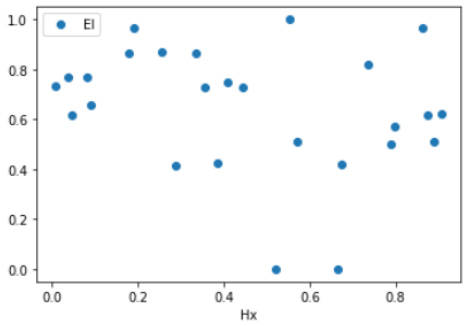


```
In [12]: sb.pairplot(df3)

         #pour faire un scatter/histogram des colonnes d'un meme dataframe, sb.pairplot permet de voir si
         #1: y a linéarité entre les 2,
         #2 : possible de les fusionner en catégories (numeric value and ordinal)?
         #3  distribution normale ?
```

```
Out[12]: <seaborn.axisgrid.PairGrid at 0x172d00f3160>
```

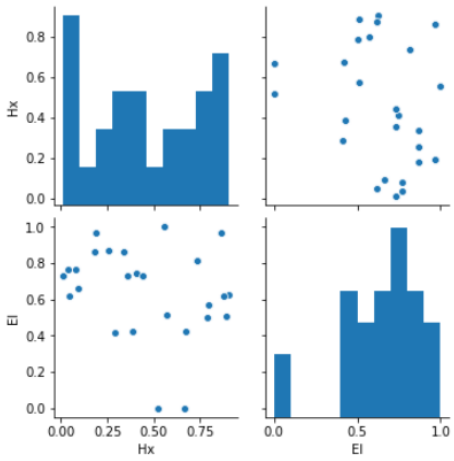

Figure 50: Python code on Jupyter Notebook for correlation plot between H(x) and EI (3/4)

```
In [13]: #On isole les colonnes qu'on veut pour réaliser un spearman correlation test
         EI = df3['EI']
         Hx = df3['Hx']

         spearmanr_coefficient, p_value = spearmanr(EI, Hx)
         print ("The correlation is %.3f" %Hx.corr(EI, method="spearman")) # avec

         The correlation is -0.301

In [15]: #test khi carré pour voir si H0  d'indépendance entre les 2 variables est vérifié , si P>0.05 on peut garder l'hypothèse nulle
         table = pd.crosstab(EI,Hx) # il faut que les variables soient dans une crosstab tab

         from scipy.stats import chi2_contingency

         chi2, p, dof, expected= chi2_contingency(table.values)

         print("Chi-square Statistic %.3f p_value %.3f" % (chi2,p))

         Chi-square Statistic 520.000 p_value 0.259
```

Figure 51: Python code on Jupyter Notebook for correlation plot between H(x) and EI (4/4)

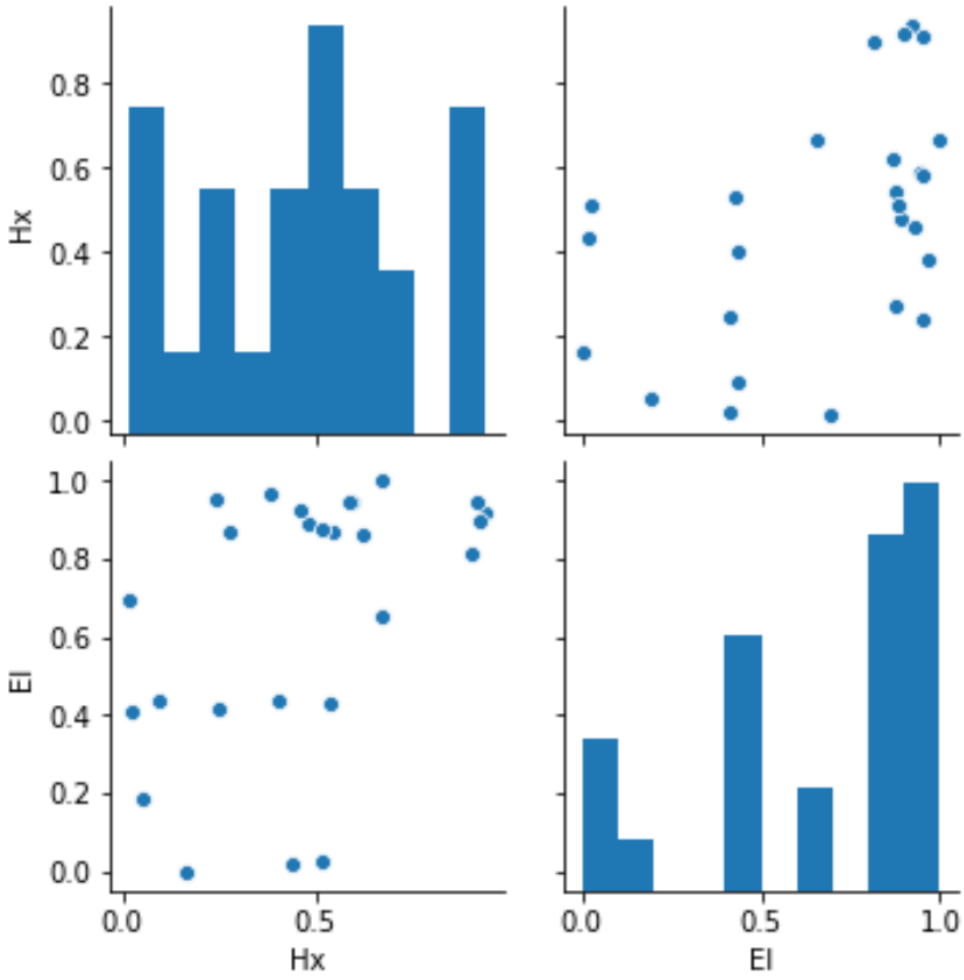

Figure 52: Distribution of EI and H(x)-12 for Youssef Lab piezometer

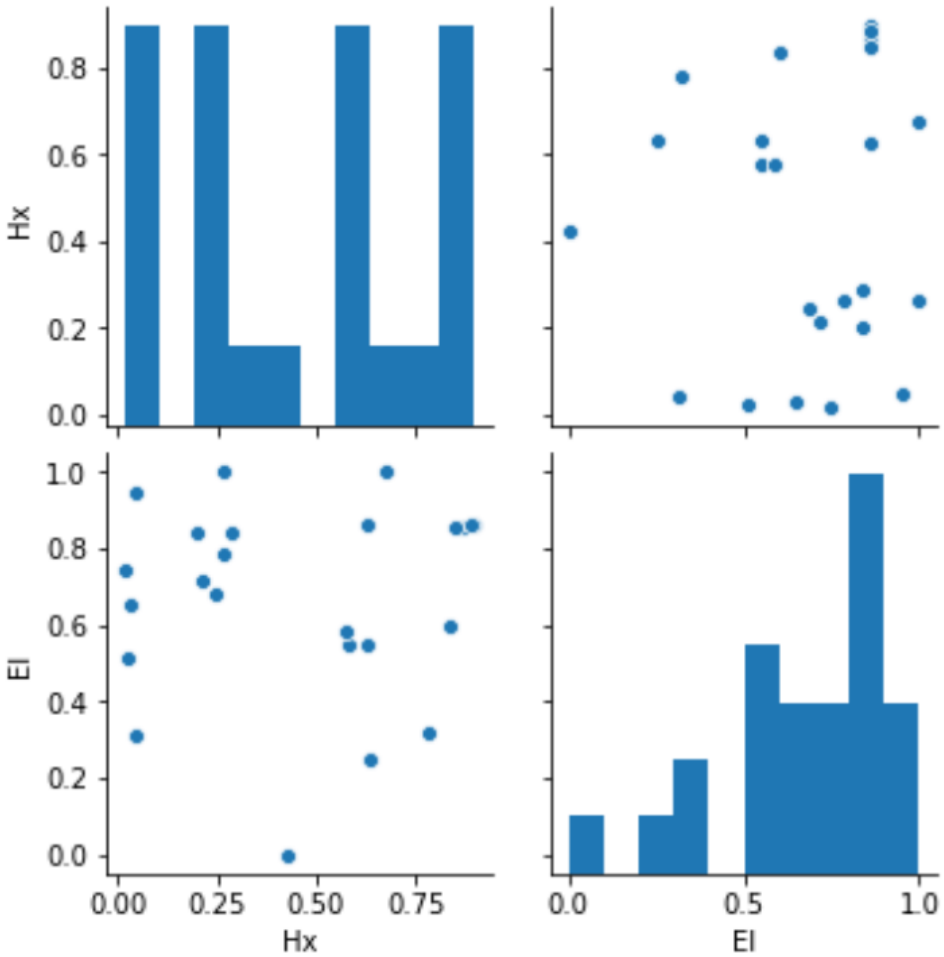

Figure 53: Distribution of EI and H(x)-12 for Amor Ben Ahmed C. piezometer

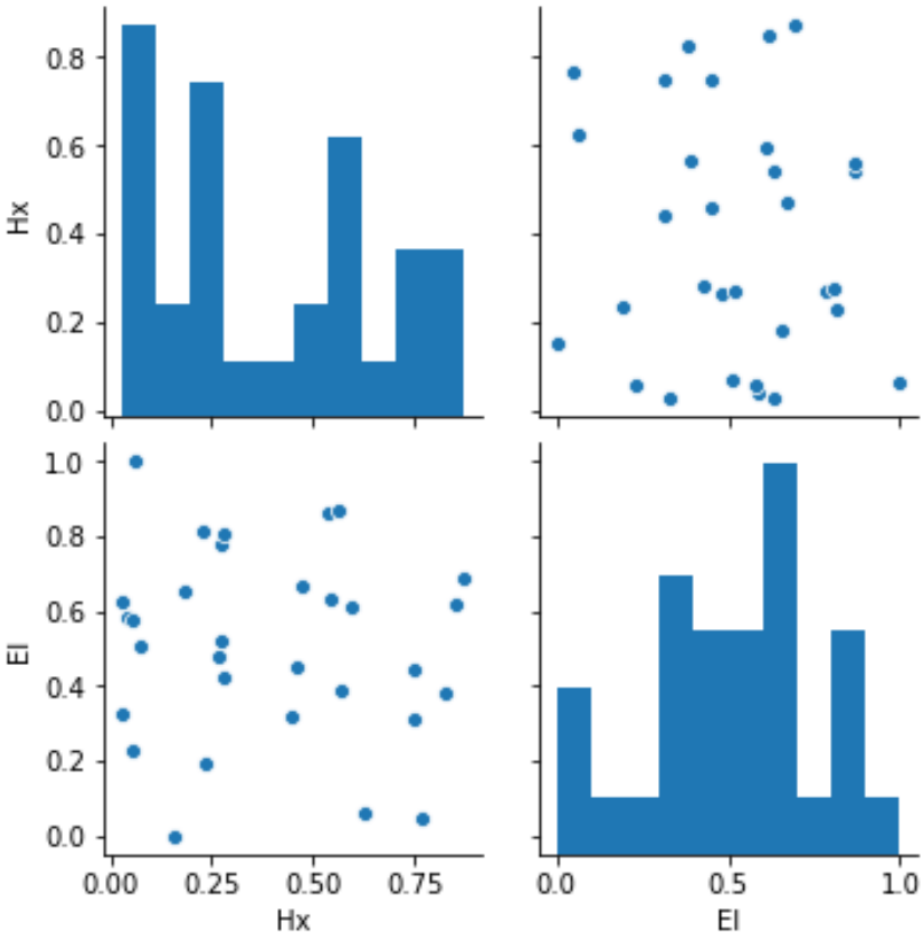

Figure 54: Distribution of EI and H(x)-12 for PZ 4343 bis/3

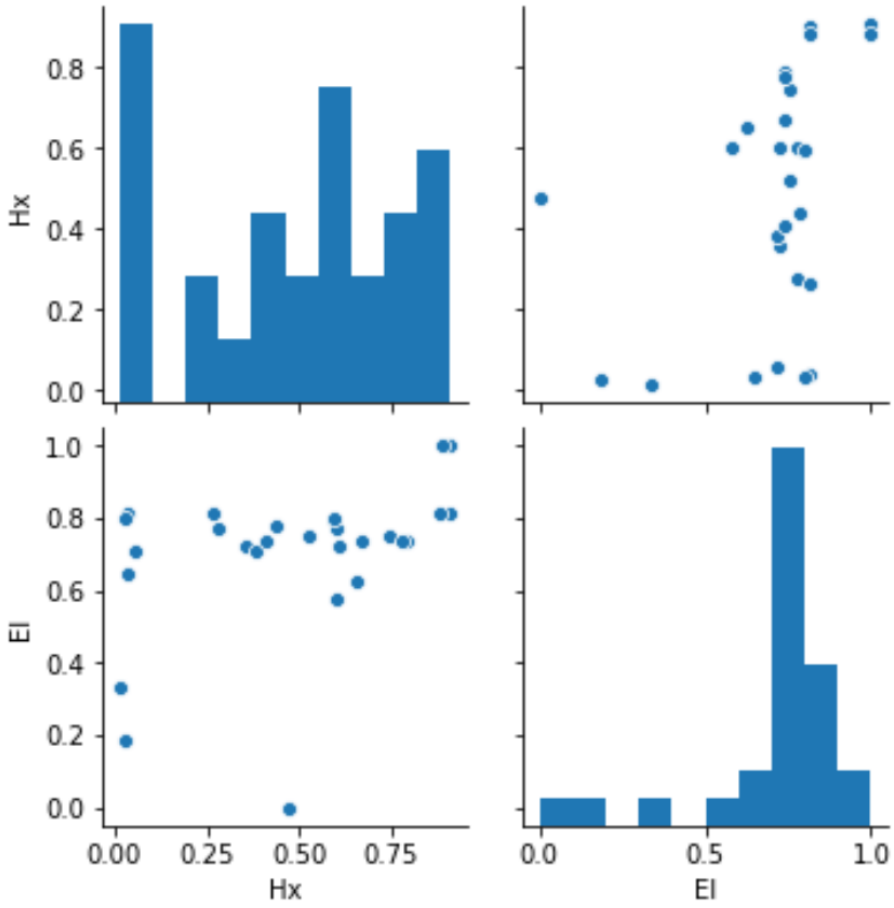

Figure 55: Distribution of EI and H(x)-12 for Salah ben A. Z. piezometer

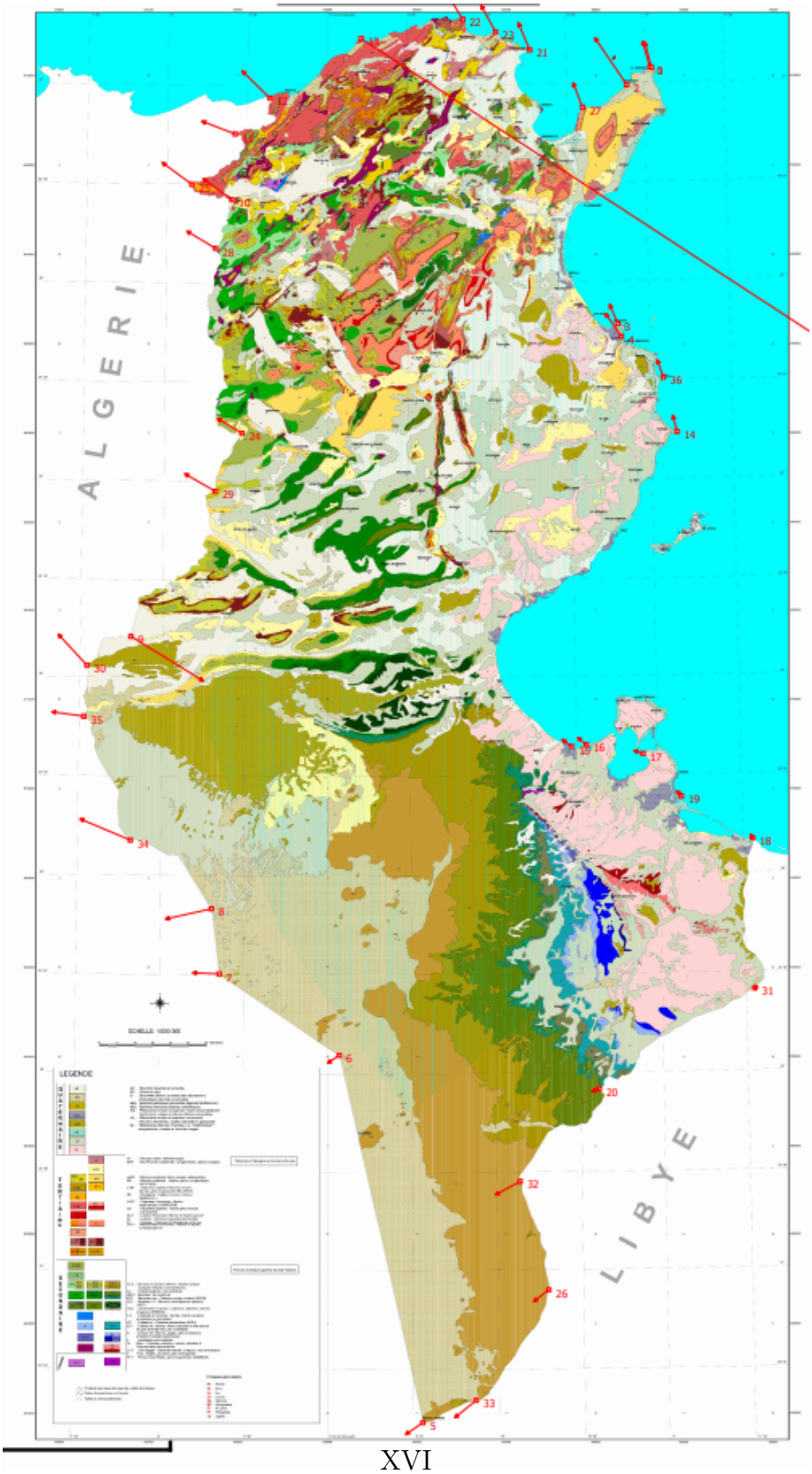

Figure 56: 1:500.000 Geological map of Tunisia

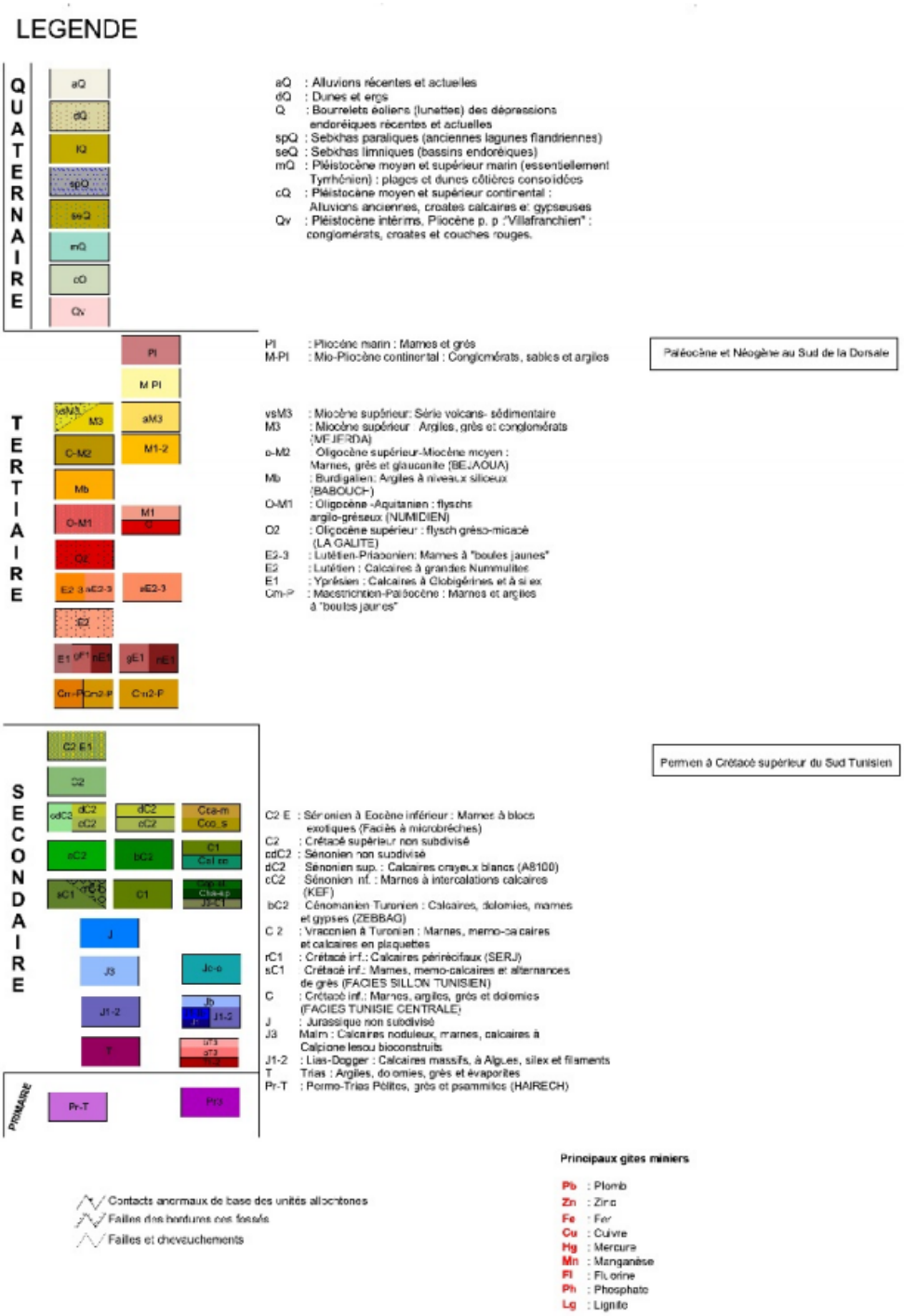

Figure 57: Legend of the 1:500.000 geological map of Tunisia

Spatio-temporal modelling of groundwater resources to improve drought risk assessments
Proposal of indicators for Siliana catchment in Tunisia

Semlali Wail

RESUME

This master's thesis proposes a monitoring system of hydrogeological droughts located in the catchment area of the Siliana river, a tributary of the Medjerda river located in northern Tunisia and dominated by farming. Three methods are adopted and propose indicators integrating groundwater resources in the diagnosis of drought over 1997-2013 period.

The first method is a meteorological based drought assessment approach using CHIRPS database providing rainfall estimates from satellite observations and in-situ stations. These data are used to calculate the Standardized Precipitation Index (SPI) and monitor monthly rainfall anomaly. Precipitation deficit at different time scales ranging from one to twenty-four months are tested to detect a direct link between rainfall deficit and groundwater storage variation.

The second method is a hydrogeological oriented approach based on in situ available piezometric data. Piezometric levels available during the low (summer) and high (winter) water seasons are normalized and provide a piezometric indicator of groundwater dynamics for each selected well. This normalized indicator is divided into water content classes.

For the last method, a hydrological model is implemented using the Soil and Water Assessment Tool (SWAT) software coupled with QGIS software and allows assessing groundwater recharge based on water infiltration. This recharge indicator is divided into volume recharge classes.

Spearman's rank correlation between SPI and piezometric indicator showed highest coefficient scores for the twelve (SPI-12) and twenty four (SPI-24) month time scales, the depth of the groundwater body apparently influencing the correlation. The confusion matrices tend to confirm the correlation analysis. In contrast, the comparisons between piezometry or meteorology drought indicators and the modelled recharge indicator showed very low result, suggesting that a hydrological model hardly represents hydrogeological dynamics.

Université catholique de Louvain
Faculté des bioingénieurs
Croix du Sud, 2bte L7.05.01, 1348 Louvain-La-Neuve, Belgique | www.uclouvain.be/agro